# Effects of sodium chloride on the mechanical strength of alkali activated volcanic ash and slag pastes under room and elevated temperatures

Pooria Ghadir [1], Hamid Reza Razeghi [1*]

[1] *School of Civil Engineering, Iran University of Science and Technology, Tehran, Iran*

[*] *Corresponding author:* E-mail address: razeghi@iust.ac.ir (H. R. Razeghi)

## Abstract

Recently, the potential of using seawater as well as sea sand in the manufacture of geopolymer concretes was investigated in several studies. Promising features in the chloride binding capacity of alkali activated cements have been observed in these experimental works. However, the mechanism of chloride binding in alkali activated cements has not yet been fully understood. In other words, the chloride binding mechanism in blended precursor systems (e.g., slag/volcanic ash) has not yet been addressed comprehensively. To this end, this study investigated effects of the sodium chloride on the microstructural and mechanical properties of alkali activated volcanic ash (VA) and ground granulated blast furnace slag as well as Portland cement pastes. In this line, unconfined compressive strength (UCS), scanning electron microscopy (SEM)-EDS-Mapping, FTIR, and XRD tests were conducted. Furthermore, effects of curing temperature on the binding capacity of chloride in alkali activated cements were examined in both elevated (HT) and room (RT) temperature conditions. The VA was replaced by slag at 0, 50, and 100 wt.%. Based on the results, samples containing 100 wt.% slag showed the highest mechanical strength in both curing conditions. Besides, addition of sodium chloride from 0 to 10 wt.% did not significantly affect the strength of samples containing 100 wt.% volcanic ash in both curing conditions. On the other hand, in HT condition, mechanical strength of samples containing 50 and 100 wt.% slag, as well as Portland cement pastes increased with increasing sodium chloride from 0 to 2.5 wt.%, and further

This is a peer-reviewed, accepted author manuscript of the following article Ghadir, P., & Razeghi, H. R. (2022). Effects of sodium chloride on the mechanical strength of alkali activated volcanic ash and slag pastes under room and elevated temperatures. Construction and Building Materials, 344, [128113]. https://doi.org/10.1016/j.conbuildmat.2022.128113

addition of sodium chloride by up to 10 wt.% led to a reduction in their strength. However, compressive strength of samples containing 50 and 100 wt.% slag, as well as Portland cement samples, decreased with the addition of sodium chloride from 0 to 10 wt.% in RT condition. Microstructural investigations were conducted, aiming to find the mechanism controlling the reactions. It was found that (N,C)-A-S-H and C-S-H gels were the dominant factor in the solidification and encapsulation of chloride ions in slag-based samples.

**Keywords**: Portland cement; Volcanic ash; Alkali activated materials; Ground granulated blast furnace slag; Sodium chloride; Curing condition.

## 1. Introduction

The existence of chloride ions in cement pastes could enhance the concerns related to the issue of rebar corrosion and undetermined durability of ordinary Portland cement (OPC) concretes [1]. Chloride ions that have penetrated the concrete can exist as either free or bound chloride ions [2]. Free chloride ions are able to diffuse through the pore solution of the concrete to reach the steel reinforcement bars and initiate steel corrosion [2]. However, the majority of the bound chloride do not contribute to the steel reinforcement corrosion [2]. In OPC concrete, the chloride ions can be chemically bound in AFm-type phases through the formation of Friedel's and Kuzel's salts as well as physically adsorbed onto the outer surfaces of calcium silicate hydrate ($Ca_2$-$SiO_4$.$H_2O$ or C-S-H) gel by Van Der Waals [3-7]. Chloride ions might be a restriction for the application of the cementitious material in reinforced concrete, even though the application prospects in soil curing or plain concrete will have been broadened [8]. Different chloride concentrations could affect the hydration mechanism and mechanical properties of OPC pastes in various ways [9-12]. The

dissolved chloride ions led to form additional unhydrated cement and less amorphous calcium silicate hydrate (C-S-H), which might be responsible for the slightly lower compressive strength of OPC mortar [10].

Alkali activated materials (AAMs) have been developed as sustainable alternative materials for OPC in the construction industry [13, 14]. It has additionally been mentioned that the carbon footprint of AAMs is much lower than that of OPC mixes [15-17]. Calcium silicate hydrate (C-S-H), calcium aluminosilicate hydrate (C-A-S-H), as well as sodium aluminosilicate hydrate (N-A-S-H) gels are the main products of alkali activated cements that were affecting the mechanical strength and chloride binding capacity of the matrix [18]. In alkali activated cements, the parameter $[Cl^-]/[OH^-]$ in the pores of the matrix as well as the parameter of the chemical composition of the gel C-(N)-A-S-H are both effective in chloride binding [19]. In another point of view, the physical and chemical properties of aluminosilicate precursor, alkali activator solution, and curing condition are the dominant factors in chloride binding capacity of alkali activated cement [20]. In previous studies, ground granulated blast furnace slag (GGBFS), metakaolin, and fly ash showed promising chloride binding ability, while silica fume did not offer suitable performance [21].

From an overall perspective, there are various opinions on chloride binding mechanisms in alkali activated cements. Some researchers believe that Friedel's salt ($C_3A{\cdot}CaCl_2{\cdot}10H_2O$) was not formed in the process of exposing alkali activated cement to chloride ions [12, 22, 23]. While, Friedel's salt was observed in sodium carbonate activated slag exposed to chloride ions [24]. In a study, sodium chloride was used as an activator for alkali activated fly ash pastes [25]. In another study, the use of seawater for the production of alkali activated fly ash-based cements was investigated [26]. In this study's alkali activated fly ash-based cement, about 86.8% of the chloride contained was encapsulated by the alkali activation process [26]. Due to the complexity of the

chloride ion function in alkali activated cements, it was theoretically predicted that the sodium ions not consumed in the alkaline activator reacted with the chloride in the structure and caused the formation of sodium chloride and deposits on N-A-S-H gel. The lack of Friedel's salt formation in alkaline activated cements containing fly ash was due to the formation of zeolite phases and the formation of N-A-S-H gel [27].

Previous research has shown that solidification/binding capacity of chloride ions in alkali activated slag cements depends mainly on the chemical phases (e.g. Layered double hydroxides (LDHs) and C-(N)-A-S-H gel) formed in these types of cements [1, 28]. The type and concentration of these phases depend on the chemical properties of slag, type and concentration of activator, temperature and alkalinity of the reaction [1, 28, 29]. Previous studies have shown that the formation of C-S-H gel due to hydration of slag led to reduced porosity and consequently a denser structure and ultimately reduced chloride ion mobility in slag-based concretes [30-32]. Also, $C_3A$ phase in the chemical composition of slag has the ability to absorb chloride ions and form Friedel's salt. Furthermore, the presence of a significant amount of magnesium ions in the chemical composition of slag led to the formation of hydrotalcite phase [33]. This phase belongs to the LDH family, which is able to absorb chloride ions from its environment due to its ion exchange capacity [34]. The results of XRD analysis showed that in alkali activated slag in the presence of chloride ion, Friedel's salt and hydrotalcite phase were formed simultaneously [33, 35].

In the preparation of fly ash-based alkali activated cements, ground granulated blast furnace slag (GGBFS or slag) is usually used as an alternative to fly ash to increase the initial strength of the samples by increasing the amount of calcium [36-39]. Similar results were observed in previous research [37, 38, 40]. Furthermore, adding slag to the mix design also reduced the penetration of chloride ions into the samples [39]. Another study found that the presence of slag reduced the

ductility of the specimens and as a result increased their stiffness and showed better resistance to deformation caused by maximum stress [41]. Chloride binding in alkali activated slag/fly ash paste was generally dependent on the physical adsorption of the reaction products and the chemical binding was not significant [22]. This study showed that C-A-S-H gel has the ability to absorb chloride physically without changing its chemical structure, while N-A-S-H porous gel has the ability to absorb chloride on the surface and pores of its cavities and sodium chloride precipitates after evaporation of water. In this study, slag was replaced by different percentages of volcanic ash (VA) (0, 25, 50 and 75 wt.% of the total weight of aluminosilicate precursor). The addition of fly ash increased porosity and permeability to chloride ions due to the formation of porous N-A-S-H gel. Meanwhile, slag-based samples (containing C-A-S-H gel) had better resistance to chloride ions than fly ash-based samples. In another study, the chloride binding capacity of N-A-S-H gel was higher than that of C-A-S-H gel [42]. Addition of fly ash to alkali activated cements led to greater physical adsorption of N-A-S-H gel due to greater contact surface area [43]. The effect of slag/fly ash ratio, $Na_2O$ concentration, silica modulus of activator and water/precursor ratio on chloride binding capacity of alkali activated slag/fly ash pastes was investigated [27]. It was observed that chloride ion chemical binding occurred in alkali activated slag samples. In other words, Friedel's salt was found only in samples containing 100 wt.% slag and its amount increased with increasing chloride ions. Chloride binding in alkali activated cements containing 100 wt.% slag was mainly due to the physical adsorption of C-A-S-H gel as well as the formation of Friedel's salt. With the addition of 20 wt.% and 40 wt.% fly ash and the formation of sodium aluminosilicate (N-A-S-H) gel, the chloride binding capacity in alkali activated slag/fly ash pastes was improved, but Friedel's salt was not observed in these samples. However, by adding more fly ash (60 wt.%

and 80 wt.%), the amount of chloride ion binding was decreased as the amount of C-A-S-H as well as N-A-S-H gels were decreased.

In alkali activated cements, the curing condition had a significant impact on compressive strength development. In this line, the results of a study on the mechanical and microstructural properties of fly ash/slag based alkali activated cement pastes showed that alkaline activation of Class F (low calcium) fly ash (FA) was not effective at ambient temperature [44]. In this study, the replacement of FA with different proportions of GGBFS (30, 50 and 70 wt.%) resulted in development of total amorphous phase content and consequently mechanical properties of paste specimens. In a study to investigate the role of curing conditions in chloride binding capacity in alkali activated fly ash paste, four types of curing conditions, including normal, oven, steam, and microwave, and three NaCl content (1, 2 and 4 wt.% of aluminosilicate precursor) were studied [20]. The results of this study showed that the application of temperature in steam curing condition accelerated the activation dissolution reactions, helped to form N-A-S-H gel and thus accelerated the geopolymer reactions that strengthen the chloride binding. However, in normal temperatures, many fly ash particles remained unreacted. Therefore, the application of temperature caused a denser structure of the geopolymer and reduced the porosity and ultimately increased the strength of the samples. Previous studies showed promising features in the chloride binding capacity of alkali activated cements. However, the mechanism of chloride binding in alkali activated cements has not yet been fully understood. In other words, the chloride binding mechanism in blended precursor systems (e.g., slag/volcanic ash) has not yet been addressed comprehensively. To this end, the present manuscript fills gaps between the available literature and sheds light on both mechanical and microstructural behavior of alkali activated volcanic ash and slag pastes elaborating the intensity of their crystalline phases using the analysis of corresponding XRD patterns in both room and

elevated temperatures. Chemical bonds structures and the variation of the amorphous bonds are further addressed using FTIR spectroscopy. SEM-EDS-mapping analysis is another part of the present study aiming at the evaluation of geopolymers' matrixes. Hence, effects of various affecting parameters including curing condition, sodium chloride content, and precursor type on the mechanical (in terms of unconfined compressive strength) and microstructural properties of alkali activated and Portland cement pastes under the effect of both hydrothermal and room curing temperatures are comprehensively investigated.

## 2. Materials and methods

### 2.1. Binders characterization

The raw materials used were ground granulated blast furnace slag (GGBFS or slag) supplied by Sepahan Cement Company and Portland cement (OPC) from Tehran Cement Company. The volcanic ash (VA) was obtained from Taftan region, Iran. The chemical compositions of the VA, slag, and OPC are shown in Table 1. Fig. 1 shows the particle size distribution of the VA, slag, and OPC assessed through laser diffraction method. Fig. 2 shows the SEM micrographs of the VA, slag, and OPC. Fig. 3 shows the XRD pattern of the VA, slag, and OPC.

NaCl powder was used in this study was purchased from Merck company with CAS number: 1.06404.1000 and 99.5% purity.

Table 1. Chemical composition of VA, slag, and OPC.

| Oxide composition | $SiO_2$ | CaO | $Al_2O_3$ | $Fe_2O_3$ | $K_2O$ | $Na_2O$ | MgO | $TiO_2$ | SrO | $SO_3$ | $P_2O_5$ | MnO | L.O.I |
|---|---|---|---|---|---|---|---|---|---|---|---|---|---|
| VA [wt.%] | 53.89 | 8.96 | 20.31 | 3.44 | 1.91 | 5.15 | 1.42 | 0.50 | 0.07 | 0.26 | 0.22 | - | 3.79 |
| GGBFS [wt.%] | 34.86 | 36.59 | 13.93 | 0.20 | 1.01 | - | 6.04 | 1.91 | 0.08 | 2.70 | - | 1.45 | 1.19 |
| OPC [wt.%] | 18.42 | 61.46 | 5.23 | 3.60 | 0.88 | - | 2.73 | 0.36 | 0.09 | 4.10 | - | 0.19 | 2.90 |

L.O.I = Loss on ignition

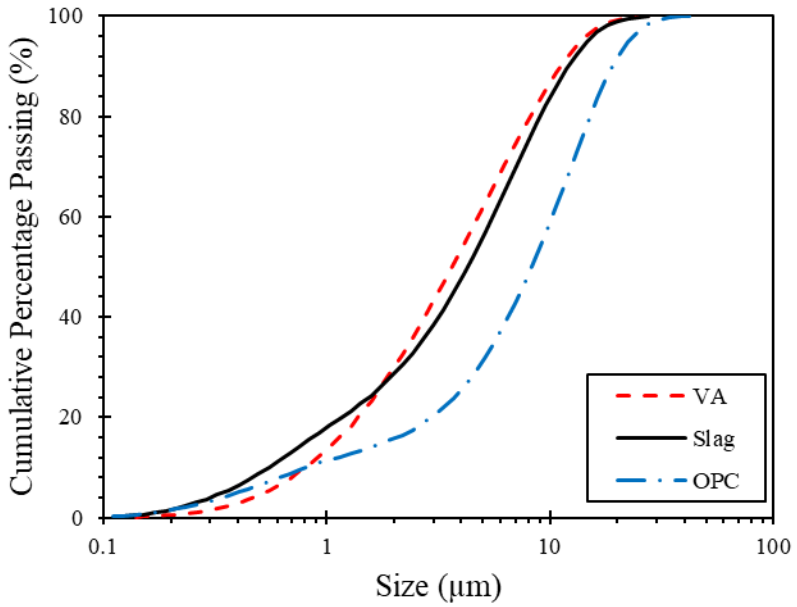


159

160 Fig. 1. Particle size distribution of VA, slag, and OPC.

161

a) b) c)

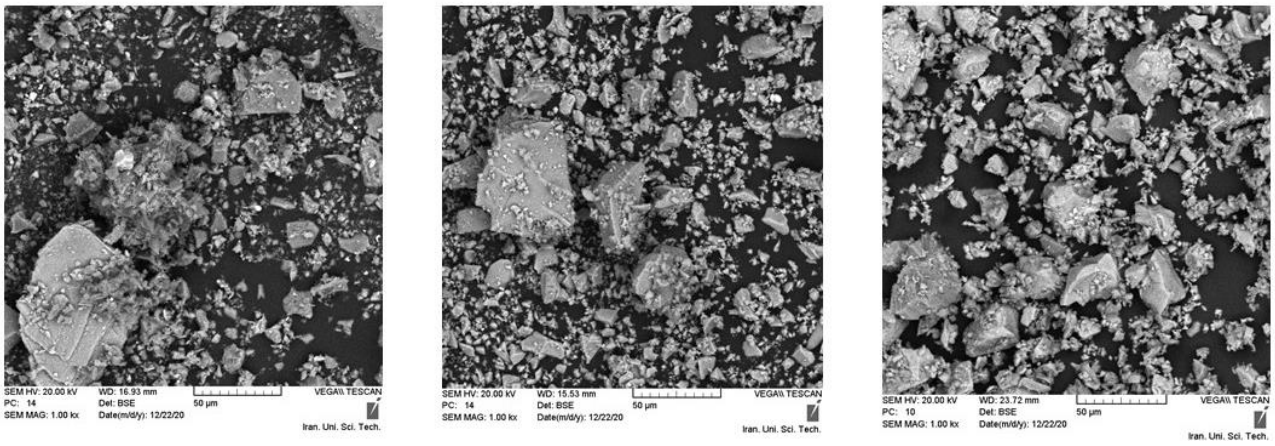

162

163 Fig. 2. The SEM micrographs of the a) VA, b) slag, and c) OPC.

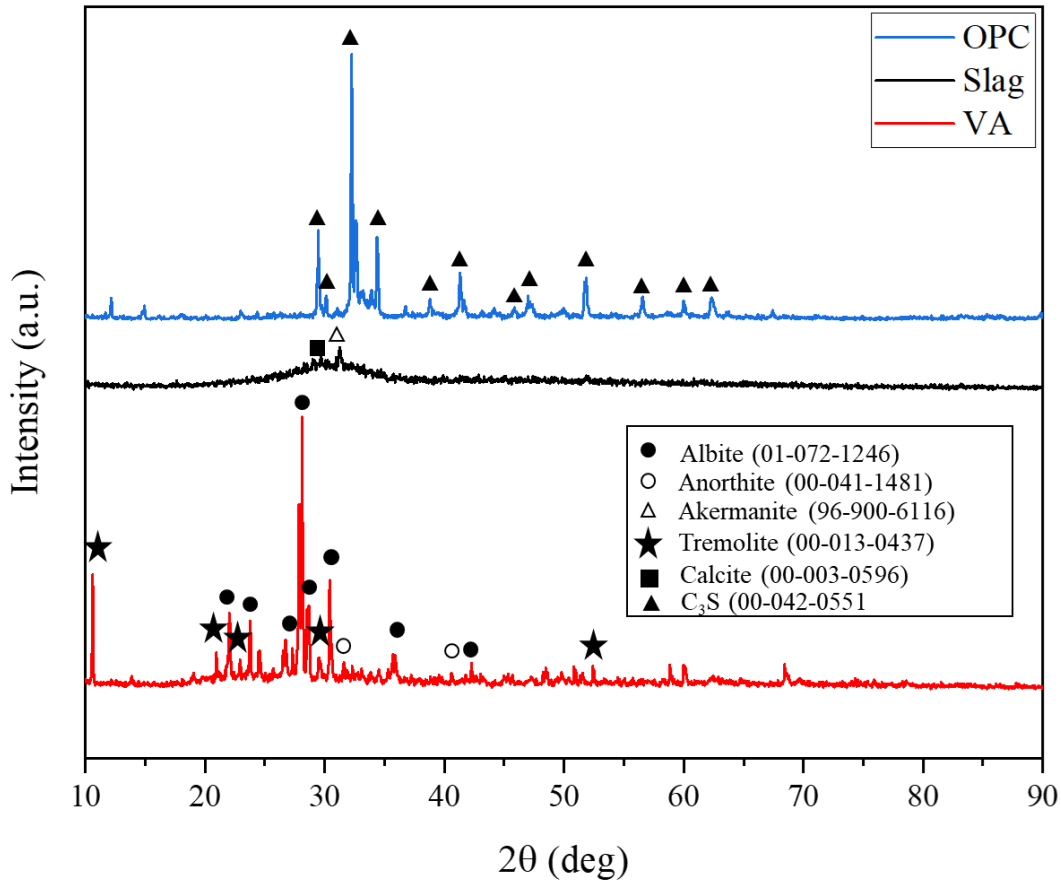


Fig. 3. The XRD spectra of the VA, slag, and OPC.

## 2.2. Alkali activator preparation

The alkali activator was prepared by mixing sodium hydroxide (NaOH) pellets of 99% purity (Merck company-CAS number:1.06482.1000) with distilled water and commercial sodium silicate ($Na_2SiO_3$) solution. The $Na_2SiO_3$ solution used in this study has a chemical composition of $SiO_2$=33.5%, $Na_2O$=14.5% and $H_2O$=52% (by mass) with a silica modulus ratio ($SiO_2$/ $Na_2O$) of 2.31. After the $Na_2SiO_3$ and NaOH solution were mixed using the laboratory's mixing equipment, the alkaline activator solution was allowed to rest for 24h before mixing with the precursors.

## 2.3. Sample preparation

VA and slag were selected as calcium aluminosilicate precursors of alkali activated pastes, and OPC was used as a reference binder. The alkali activator was prepared by mixing NaOH solution and commercial $Na_2SiO_3$ solution.

To prepare alkali activated pastes, after premixing the raw materials for 1 min, the prepared alkali activator solution was added to the specified amounts of precursors and mixed for 5 minutes by hand mixing. OPC pastes were prepared through mixing distilled water with given amounts of Portland cement. The process of mixing was performed according to ASTM C305-14 [45]. Water/cement ratio was kept constant for both alkali activated/Portland cement systems to ensure suitable homogeneity and workability. This ratio was 0.28 and 0.35 for Portland cement and alkali activated specimens, respectively. Previous studies investigated the effect of $Na_2O$ concentration and silica modulus on the mechanical strength of alkali activated volcanic ash and slag pastes [46]. In this line, $Na_2O$ content was 8 wt.% of binder and silica modulus was 1.5 for alkali activated specimens. In alkali activated specimens, the VA was replaced by slag at 0, 50, and 100 wt.% to study the effects of different replacement levels on the mechanical and microstructural properties of alkali activated pastes, Table 2. To investigate the effect of NaCl on mechanical strength of cementitious systems, NaCl was mixed with binder in dry state (0, 2.5, 5, and 10 wt.% of binder), Table 2. In the next step, the fresh homogenous pastes were cast into cubic Teflon molds of the size 20×20×20 (±0.3 mm) mm for the uniaxial compressive strength test. A plate vibrator was used for densification of pastes for 60 seconds. After casting, for alkali activated and Portland cement pastes, the molds were placed in a plastic container with a nearly constant relative humidity (RH) of 95 ± 2% and temperature of 25 ± 2 °C for 24h. When the 24h period was finished, specimens were taken out of molds. Both of alkali activated and Portland cement specimens were cured using two different curing regimes: 1) In a humid container with RH=95 ± 2% and elevated temperature

(50 ± 2 °C) for 24h. 2) In a humid container with RH=95 ± 2% at room temperature (25 ± 2 °C) for 7, 28 and 90 days. Summary of the test schedule is given in Table 3. The Portland cement mechanical tests were done for benchmarking purposes.

Table 2. Mixture proportion of cementitious systems.

| Series | W/C | Slag replacement (wt.%) | NaCl content (wt.% of binder) |
|---|---|---|---|
| Alkali activated | 0.35 | 0, 50, 100 | 0, 2.5, 5, 10 |
| Portland cement | 0.28 | - | 0, 2.5, 5, 10 |

Table 3. Summary of the test schedule.

| Series | Curing condition | Curing time |
|---|---|---|
| Alkali activated | HT* | 24 h after 1 day precuring |
| Alkali activated | RT¥ | 7, 28, 90 days |
| Portland cement | HT | 24 h after 1 day precuring |
| Portland cement | RT | 7, 28, 90 days |

* Temperature = 50 ± 2 °C, relative humidity = 95 ± 2%
¥ Temperature = 25 ± 2 °C, relative humidity = 95 ± 2%

## 2.4. Mechanical properties

Uniaxial compressive strength (UCS) test was performed by means of a universal testing machine with a 50 kN load cell attached and constant strain rate of 0.5 mm/min according to ASTM C109 [47]. Three specimens were utilized in each measurement, and the average of the measured compressive strengths was reported.

## 2.5. Microstructure characterization

The particle size distributions of VA, slag, and OPC, shown in Fig. 1, were determined through laser diffraction method by a laser particle size analyzer (CILAS 1190).

The chemical compositions of the VA, slag, and OPC, shown in Table 1, were analyzed by using X-ray fluorescence (XRF) spectroscope (PANalytical Axios mAX).

Microstructural characterization was carried out on RT-90 days and HT cured alkali activated paste specimens.

The X-Ray Diffraction (XRD) patterns measurement was carried out to examine the crystalline phases in the pastes using a D8 ADVANCE (Bruker company, Germany) using Cu Ka radiation (k = 1.54056 Å), operated at 40 kV and 30 mA with a step size of 0.04 deg and a scanning rate of 0.15 deg $s^{-1}$ in the 2θ range of 10–90º.

Fourier transform infrared (FTIR) spectroscopy analysis was conducted using a Perkin Elmer System series 2000 spectrophotometer (Spectrum RXI) in a wave number range of 450 to 4400 $cm^{-1}$ with a resolution of 2 $cm^{-1}$ to identify the functional groups of alkali activated cements.

Scanning electron microscopy (SEM) was used to observe the specimens' morphology using the FEI ESEM QUANTA 200 device together with elemental mapping spectroscopy (EDS Silicon Drift 2017).

## 3. Results and discussion

### 3.1. Unconfined compressive strength (UCS) test results

#### 3.1.1. UCS in HT curing condition

Fig. 4 presents the effect of NaCl addition on compressive strength of alkali activated and Portland cement specimens in HT curing condition.

The replacement of volcanic ash with slag from 0 to 100% by weight of the precursor led to an increase in mechanical strength (Fig. 4a-c). Similar results were observed in previous research [36-39]. The inclusion of slag may aid in the completion of the reaction, resulting in increased strength. As a result of the increased Ca and Si contents provided by slag and sodium silicate materials, high compressive strength is found, which is caused by the lesser availability of pores, which influences

compact structure [44]. Noteworthy, samples containing 50 and 100 wt.% slag showed higher strength than Portland cement samples.

In samples containing 100 wt.% volcanic ash (VA-based samples), with increasing the percentage of sodium chloride from 0 to 10 wt.%, the mechanical strength of the samples was almost constant. While in samples containing 50 and 100 wt.% slag, with increasing the amount of sodium chloride from 0 to 2.5 wt.%, the mechanical strength was increased, and further sodium chloride by up to 10 wt.% reduced the strength of the samples.

Previous research showed that NaCl was found to act as an accelerator or retarder for alkali activated slag mortars [8, 12]. The results showed that NaCl at low levels (up to 4 wt.%) act as an accelerator but as a retarder at the high concentrations [12]. A certain amount (2 wt.% of the binder) of NaCl was added into the slag composite matrix geopolymer to increase its early strength (3-day) and late strength (28-day) [8]. In other words, NaCl can be employed as an activator because the sodium ions in it can offer a more alkaline environment for slag hydration, and the chloride ions can also participate in the reaction to generate some crystals [25, 48, 49]. On the contrary, the strength of the samples began to decline as the amount of NaCl in the mixture increased from 2 wt.% to 4 wt. % [8].

Previous research showed that the application of temperature improved the physical and chemical absorption of chloride ions in the alkali activated cement gel structure [20, 50]. Because with increasing temperature, the level of N-A-S-H gel for adsorption of chloride ion increased. However, the rapid evaporation of the alkaline activator in oven curing condition caused microstructural cracks and dry shrinkage, which led to the cessation of the geopolymer process and the reduction of mechanical strength compared to steam curing condition. On the contrary, in

steam curing condition, the presence of steam prevented the shrinkage process from drying out, and the strength of the samples was not reduced.

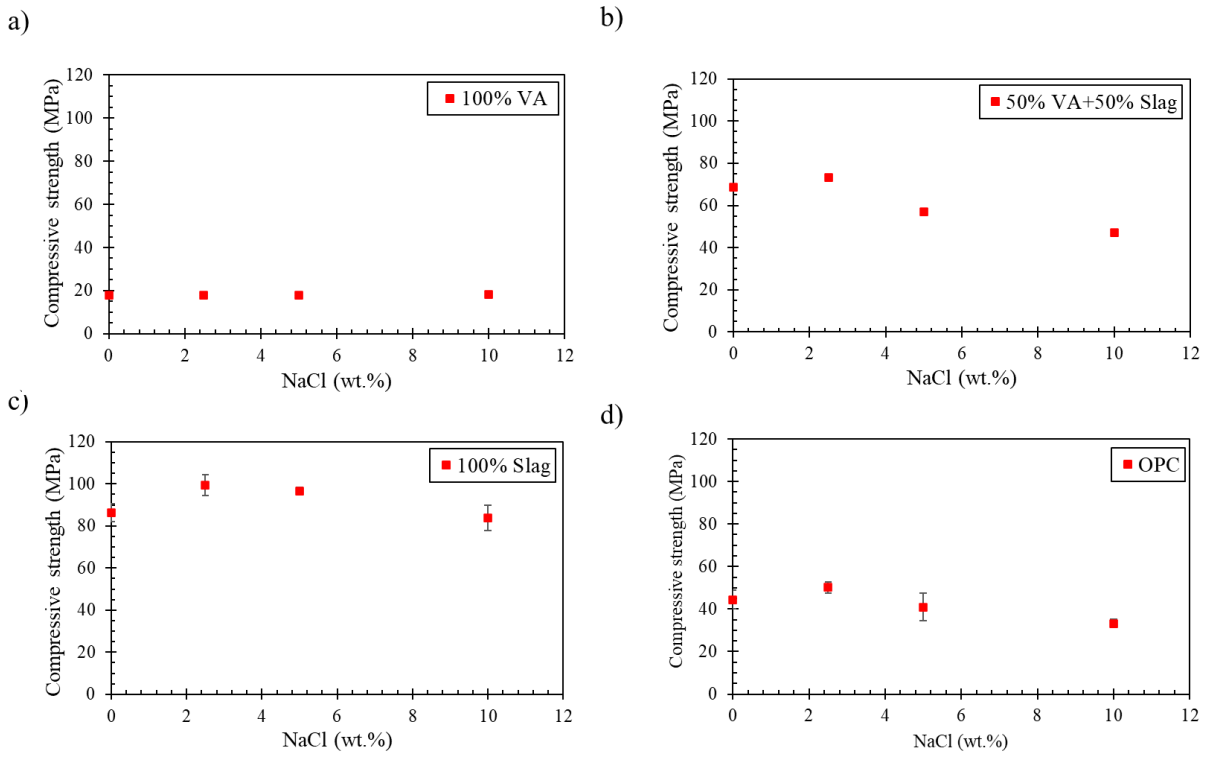


Fig. 4. Effect of NaCl addition on compressive strength of a) alkali activated (100 wt.% VA), b) alkali activated (50 wt.% VA+50 wt.% slag), c) alkali activated (100 wt.% slag), and d) Portland cement pastes in HT condition.

### 3.1.2 UCS in RT curing condition

Fig. 5 shows the effect of NaCl addition on compressive strength of alkali activated and Portland cement specimens in RT curing condition.

In RT condition, replacing volcanic ash with slag showed similar trend as in HT condition. Furthermore, samples containing 50 and 100 wt.% slag showed higher strength than Portland cement pastes.

The strength of VA-based samples was almost constant over time. In other words, at low curing temperatures, VA-based samples required a long curing time to sufficiently and efficiently dissolve the aluminosilicate elements and complete the polycondensation process to achieve appropriate compressive strength. In addition, the extended curing time can bring about greater homogenous microstructure, perfect dissolution of aluminosilicate gel, and consequently the huge quantity of reacted particles. The mechanical strength of geopolymer concrete samples made from fly ash (low in calcium) showed that room temperature was unsuitable for curing of these samples because the strength development was prolonged [51].

While in samples containing 50 and 100 wt.% slag and Portland cement pastes, the humidity in the environment led to a significant increase in mechanical strength. In samples containing Portland cement, the presence of moisture contributed to the hydration reaction which increased the strength of the samples over time [10].

In VA-based samples, with increasing the percentage of sodium chloride from 0 to 10 wt.%, the strength of 7-day and 28-day samples was increased slightly, while the strength of 90-day samples was declined gradually.

In samples containing 50 and 100 wt.% slag, increasing the amount of sodium chloride from 0 to 5 wt.% decreased the strength of 7, 28 and 90 day samples and added NaCl up to 10 wt.% not affected the mechanical strength considerably.

In Portland cement specimens, the strength of 7-day samples (short-term strength) was increased with the increasing amount of sodium chloride (up to 5 wt.%) and the further increasing amount of sodium chloride up to 10 wt.%, declined the mechanical strength. Similar results have been observed in previous research [9, 10]. In comparison, the 90-day (long-term) strength of Portland

cement pastes was decreased with the addition of sodium chloride (up to 5 wt.%) and then remained almost constant.

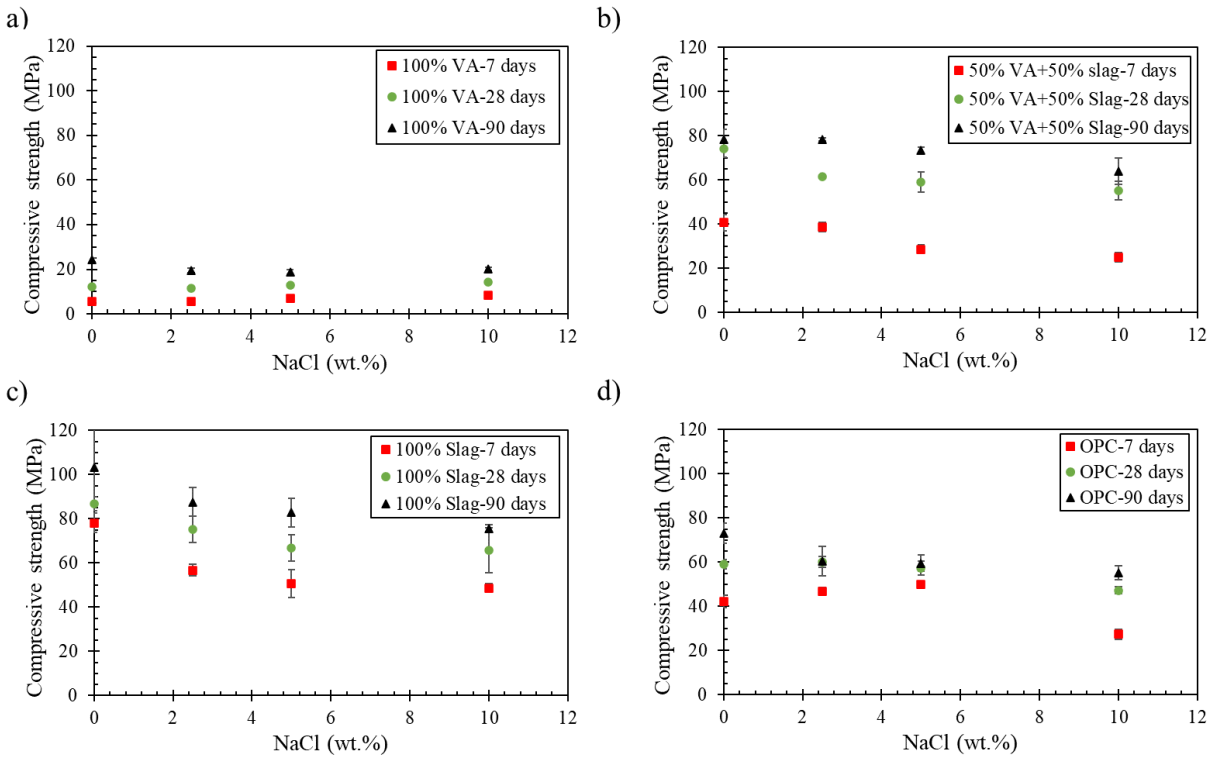


Fig. 5. Effect of NaCl addition on compressive strength of a) alkali activated (100 wt.% VA), b) alkali activated (50 wt.% VA+50 wt.% slag), c) alkali activated (100 wt.% slag), and d) Portland cement pastes in RT condition.

### 3.1.3 The effect of curing condition on UCS

Fig. 6 shows the effect of NaCl addition and curing condition on compressive strength of pastes simultaneously.

The strength of cured samples in HT condition (after 1 day) was almost comparable to that of samples cured at RT (after 90 days). Curing conditions provided a vital contribution to the compressive strength development of alkali activated cement pastes. In general, high curing temperature in HT condition enhanced reactivity of aluminosilicate precursors in alkaline

environments earlier than RT condition [52, 53]. In other words, increasing the curing temperature facilitated the dissolution of silica and alumina bonds in alkaline environments, which led to increased formation of geopolymeric bonds and thus higher strengths [53, 54]. Some previous research showed that the thermal curing process is necessary for alkali activation of aluminosilicate raw materials [55-57]. However, geopolymerization reactions of raw materials rich in calcium content occurred at ambient temperature [58].

In HT curing condition, the presence of temperature and humidity simultaneously contributed to the hydration process of slag and Portland cement particles. Therefore, the rate of strength development for samples containing slag or Portland cement in this curing condition was much higher than in the RT condition. Furthermore, in samples containing slag, heat treatment increased the rate of dissolution, hydrolysis, and polycondensation of the alkali activated cement in the early stages of curing.

The geopolymerization process requires structural water (crystalline water), which creates an environment for the dissolution and hydrolysis of precursors and enables the transfer of ions [14, 20, 59]. Besides, there is another water in the system called physical water (free water), which negatively affects mechanical strength. Free water is used only due to increased workability in the system [14, 20, 59]. The reason for the similar strength of samples containing volcanic ash in both curing conditions was that the high humidity of the environment prevented the evaporation of free water of the geopolymer [14, 20, 59]. Therefore, the alkalinity of the matrix increased slowly. As a result, it slowed down the geopolymerization rate in both dissolution and hydrolysis stages, and the compressive strength increased slowly.

In both curing conditions, samples containing 100 wt.% slag were leading at compressive strength, followed by samples containing 50 wt.% slag, Portland cement, and 100 wt.% volcanic ash.

Therefore, it can be seen that the addition of slag or the addition of CaO in the precursor led to higher mechanical strength of alkali activated cement than Portland cement against the addition of chloride ions in both curing conditions.

As can be seen, the addition of sodium chloride from 0 to 10 wt.% did not significantly affect the strength of VA-based samples in both HT and RT conditions. However, in HT condition, the mechanical strength of samples containing 50 and 100 wt.% slag as well as Portland cement pastes increased with increasing sodium chloride from 0 to 2.5 wt.%, and further addition of sodium chloride by up to 10 wt.% led to mechanical strength reduction. The previous research showed that NaCl at low levels (up to 4 wt.%) act as an accelerator but as a retarder at the high concentrations for alkali activated slag mortars [8, 12]. On the other side, in RT condition, the strength of samples containing 50 and 100 wt.% slag as well as Portland cement samples decreased with the addition of sodium chloride from 0 to 10 wt.%.

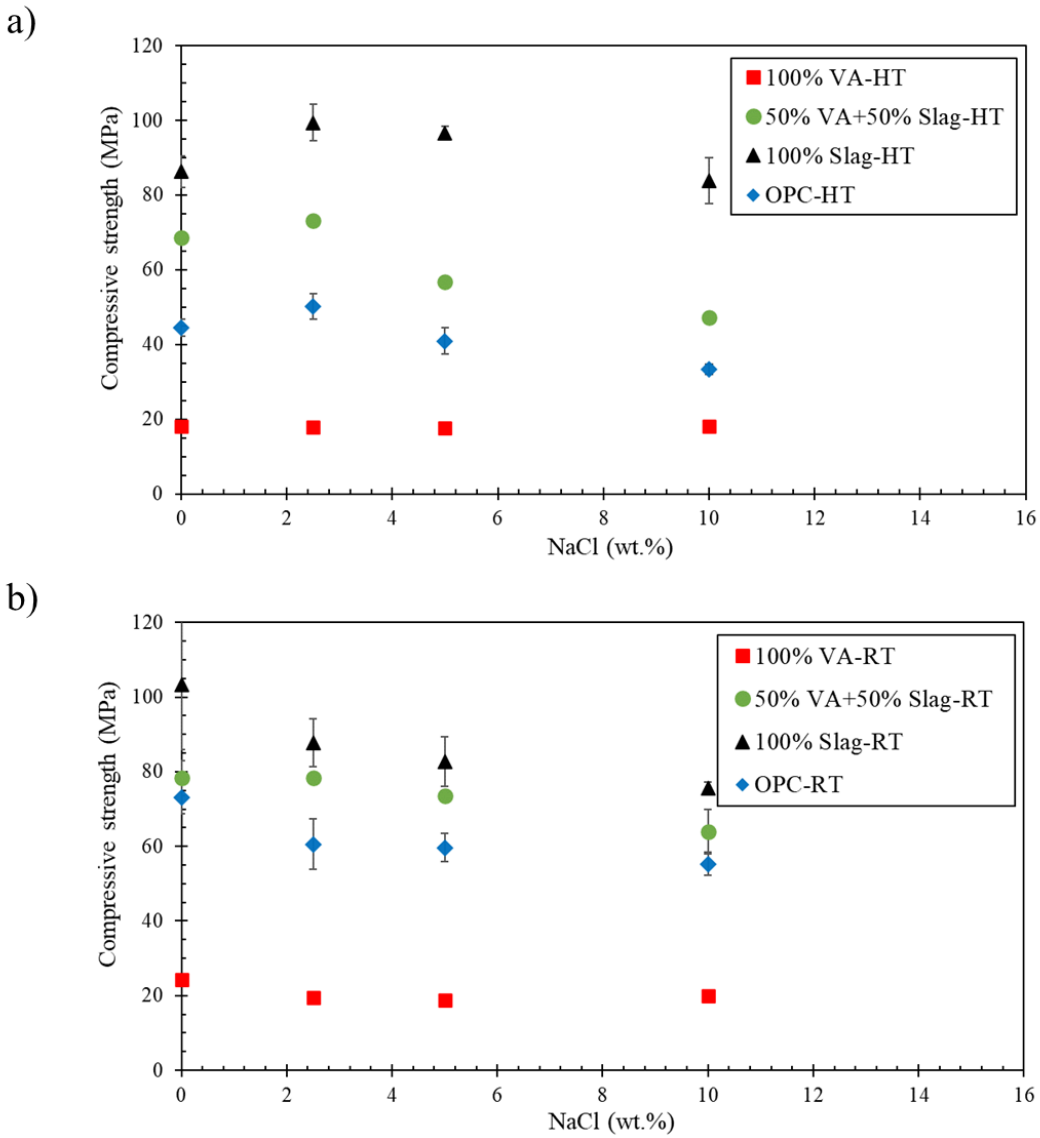


Fig. 6. Effect of NaCl addition and curing condition on compressive strength of alkali activated (100 wt.% VA, 50 wt.% VA+50 wt.% Slag, 100 wt.% Slag) and Portland cement pastes in a) HT condition and b) RT (90 days) conditions.

## 3.2. Microstructural analysis

### 3.2.1. XRD analysis

The crystalline phases of alkali activated cement pastes were identified using the XPert High Score software, Fig. 7.

354 The intensity of peaks obtained in VA-based samples was stronger than slag-based samples, which
355 could be due to the crystalline structure of volcanic ash compared to slag [60-62]. Because slag is
356 a material with an amorphous phase, it is easier to activate it at ambient temperature than volcanic
357 ash, while a large part of volcanic ash is crystalline phase, and it requires higher temperatures
358 around 50 ºC to 100 ºC to activate [60-62]. In addition, the $CaO/SiO_2$ content of volcanic ash is
359 significantly lower than that of slag, meaning that volcanic ash contains a small amount of CaO
360 but is rich in silica and alumina, whereas in the case of slag it is the opposite [60-62]. In general,
361 if more reactive calcium is present in the chemical composition of the precursor, pozzolanic
362 reactions occur more rapidly especially in existence of water. Another possible reason for the
363 strength increment due to the increase in slag is that the reaction of slag and alkaline solution is an
364 exothermic process, which in turn improves the geopolymerization process [63].

365 Alkaline activation of slag formed both calcium silicate hydrate (C-S-H) and calcium
366 aluminosilicate hydrate (C-A-S-H), meanwhile, alkaline activation of volcanic ash produced
367 sodium aluminosilicate hydrate (N-A-S-H). $Na_2O$-CaO-$Al_2O_3$-$SiO_2$ or (N,C)-A-S-H gel was
368 formed by activating the combination of slag and volcanic ash. Combining high calcium precursors
369 with low calcium ones caused the simultaneous and synergistic formation of C-A-S-H and N-A-
370 S-H gels, strengthening the mechanical properties of matrix. (N,C)-A-S-H gel is a mechanically
371 strong gel made of a combination of crystalline and amorphous structures with a high
372 concentration of silica which caused better microstructural density of the samples [64-67].

373 As shown in the Fig. 7, after the geopolymerization reactions, the type of crystalline phases of
374 alkali activated cements remained almost the same compared to the raw materials. However, the
375 intensity and type of the amorphous phase were considerably altered. Origin Pro software was
376 used to compare the crystallinity index (CI) of the samples, Fig. 8. The results showed the amount

of crystalline phase in VA-based samples cured in RT condition was higher than samples cured in HT condition. While in slag-based samples, the amount of amorphous phase was higher in RT curing condition. It can be concluded that the addition of slag to the samples led to a growth in the amorphous phase and a reduction in the crystalline phase, which has been observed in previous studies [68]. This has caused the compressive strength of the samples to undergo a rise with increasing slag content in the precursor. In another point of view, the amount of crystalline phase in VA-based samples increased by adding NaCl under HT curing condition, while ambient temperature showed the opposite trend. Therefore, the reason for the similar mechanical strength of VA-based samples with various sodium chloride contents in HT condition can be attributed to the compaction of the crystalline structure of these samples. In samples containing slag, the amount of crystalline phase increased with the addition of sodium chloride in both curing conditions.

The XRD pattern of VA-based samples in both curing conditions and two states with and without NaCl was similar to raw volcanic ash. However, the decrease in intensity of some crystalline peaks due to the formation of amorphous phases was due to the addition of an alkaline activator. By adding sodium chloride, some of the crystalline peaks decreased in intensity compared to the sample without NaCl, and some of the other peaks increased in intensity. This has prevented the reduction of mechanical strength by adding sodium chloride to the samples. Chabazite-Ca zeolite and N-A-S-H gel were clearly visible in samples containing volcanic ash. Besides, sodium chloride (halite phase) was detected in samples containing sodium chloride [1]. Sodium aluminum silicate hydrate (N-A-S-H) with card number 00-038-239 was the same as zeolite Y phase. This phase became more intense as the amount of sodium chloride increased. Previous studies showed that N-A-S-H gel did not have much effect on the chemical adsorption of chloride and absorbed more chloride ions by surface adsorption [1].

In slag-based samples, (N,C)-A-S-H and C-S-H gels were visible in their XRD patterns which play a significant role in increasing the mechanical strength of samples compared to samples without slag [69]. Also, these gels were the main factor in the solidification and encapsulation of chloride ions in their dense structure. Friedel's salt and also sodium chloride phases were also observed in samples containing sodium chloride. In samples containing 100 wt.% slag, amorphous geopolymer gels were formed in RT curing condition, while in HT curing condition, the structure tended to crystallize. Noteworthy, low content of MgO in slag, as well as insufficient pore spaces for hydrotalcite precipitation may lead to nuance formation of hydrotalcite phase which was not detected in XRD analysis [1].

In general, the elements magnesium, calcium and aluminum in slag led to the formation of Cl-hydrotalcite or (Mg-Al LDH) and also the formation of Cl-hydrocalumite or (Ca-Al LDH) [70]. Both hydrotalcite and hydrocalumite compounds have an LDH structure that encapsulated chloride anions in their interlayer structure. High content of CaO in slag played a significant role in Ca-Al-LDH formation that resulted in Friedel's salt [1, 71]. Recent studies investigated the effect of metakaolin and limestone as additives to alkali activated slag pastes to enhance binding chloride capacity through Ca-Al-LDH and consequently Friedel's salt formation [1, 71]. Physical adsorption of chloride ions can occur by the double electrical layer on the outer surface of LDHs with a positive charge.

In Portland cement, the chemical adsorption of chloride ions depends on Friedel's salt. Meanwhile, the adsorption mechanism of chloride ions in alkali activated slag includes physical adsorption by C-S-H gel and chemical adsorption by Cl-hydrocalumite and Cl-hydrotalcite [70].

(N,C)-A-S-H gel and C-S-H gel were also detected in samples containing both volcanic ash and slag. Friedel's salt also played an important role in the chemical adsorption of chloride ions in these samples.

424 a)

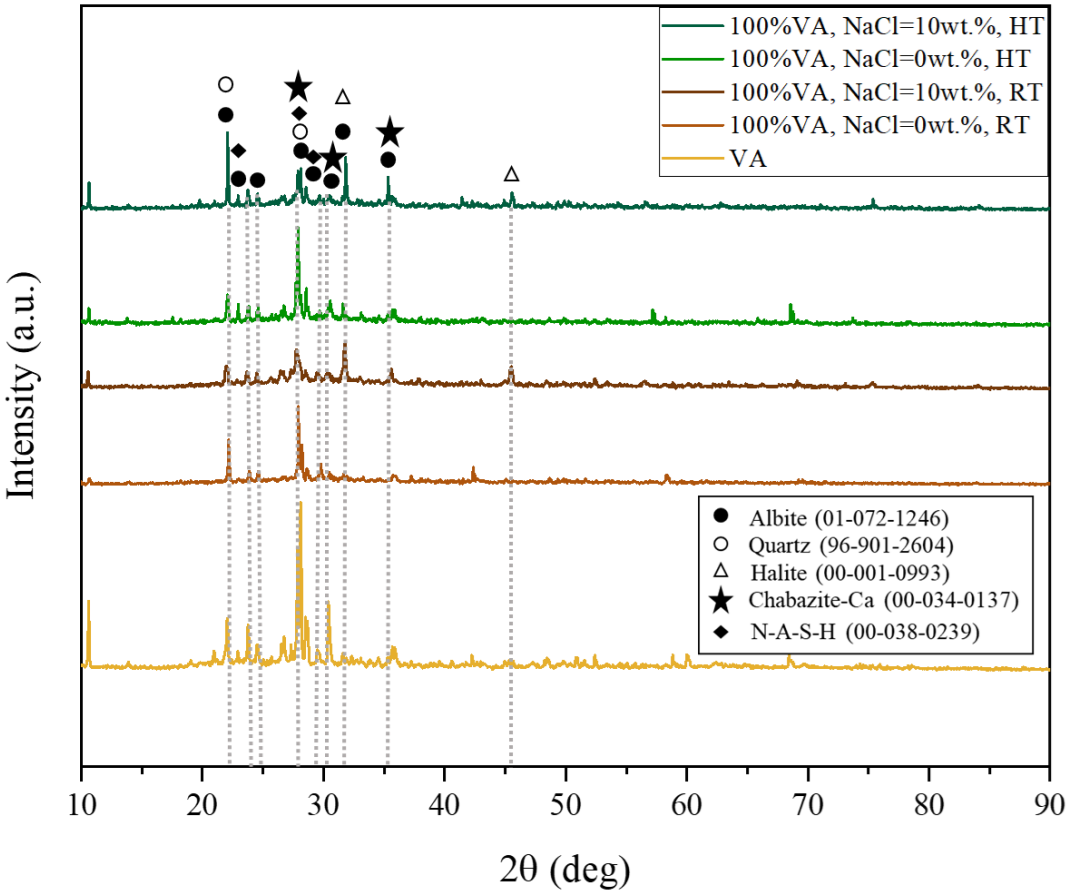


425

426 b)

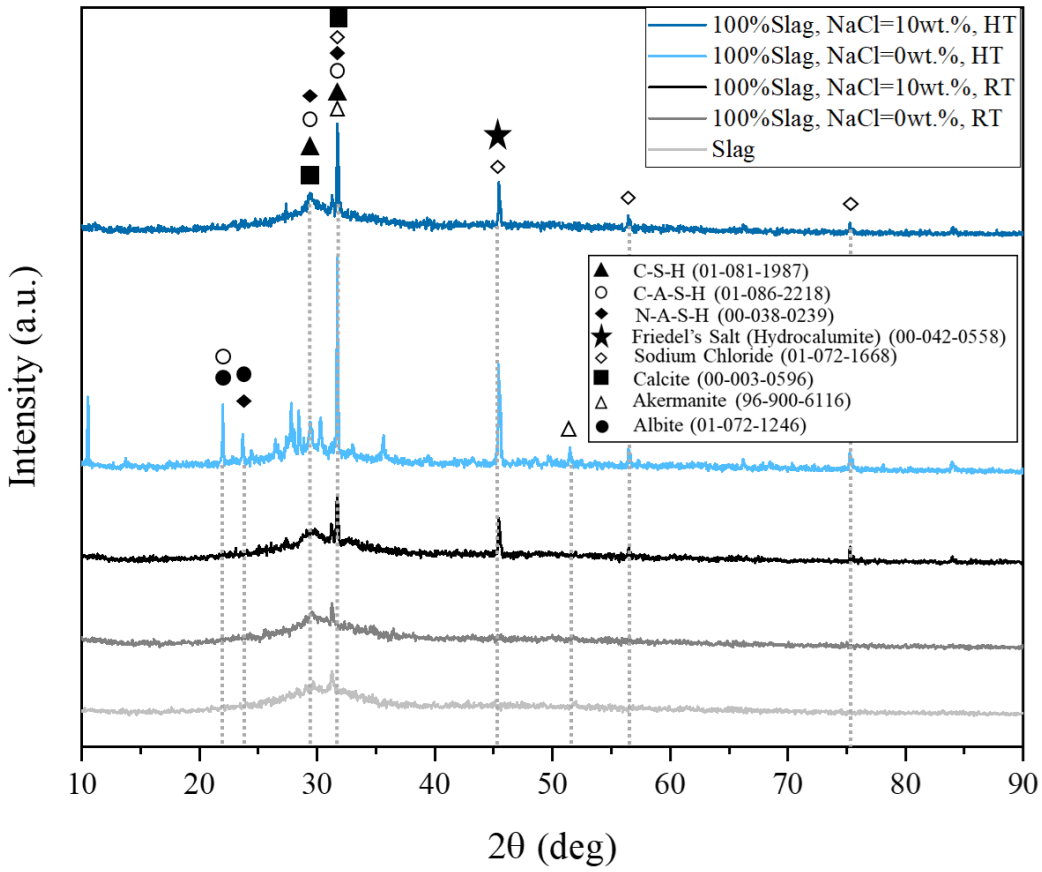
100%Slag, NaCl=10wt.%, HT
100%Slag, NaCl=0wt.%, HT
100%Slag, NaCl=10wt.%, RT
100%Slag, NaCl=0wt.%, RT
Slag
C-S-H (01-081-1987)
C-A-S-H (01-086-2218)
N-A-S-H (00-038-0239)
Friedel's Salt (Hydrocalumite) (00-042-0558)
Sodium Chloride (01-072-1668)
Calcite (00-003-0596)
Akermanite (96-900-6116)
Albite (01-072-1246)
Intensity (a.u.)
10
20
30
40
50
60
70
80
90
2θ (deg)

427

428 c)

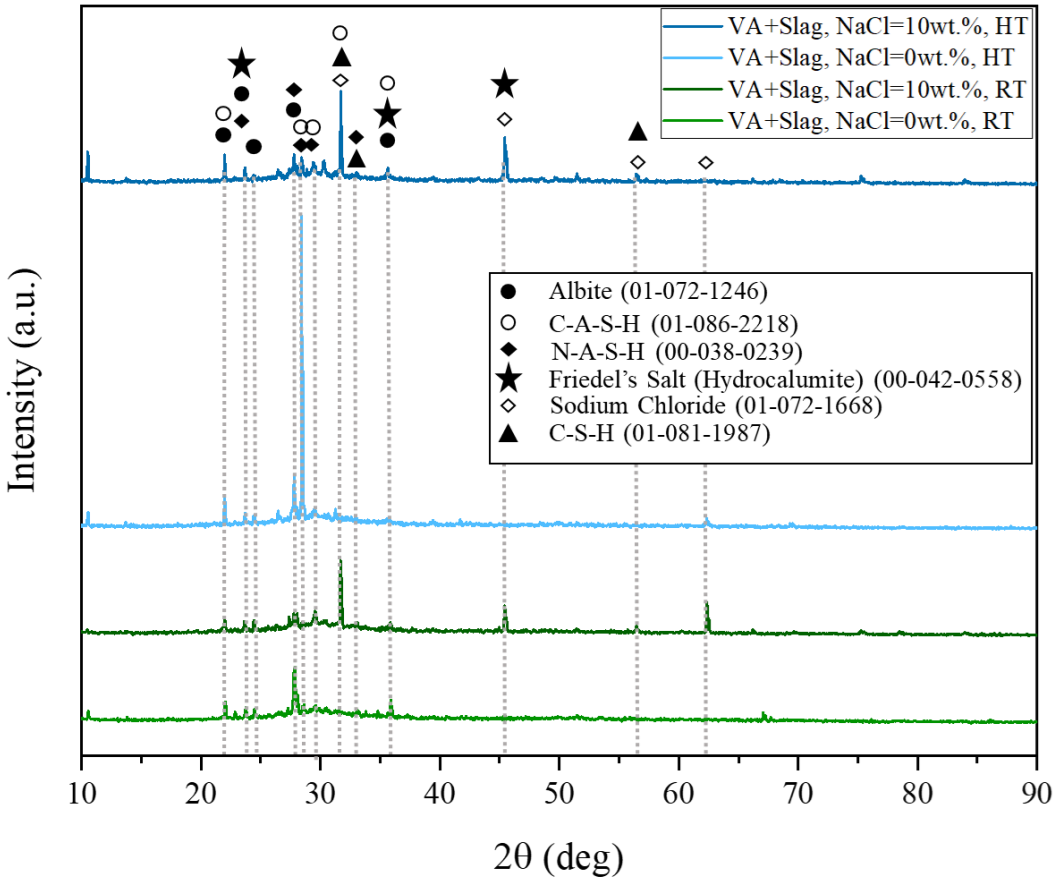


Fig. 7. XRD patterns of the a) alkali activated (100 wt.% VA), b) alkali activated (100 wt.% slag) c) alkali activated (50 wt.% VA+50 wt.% slag), in HT and RT conditions.

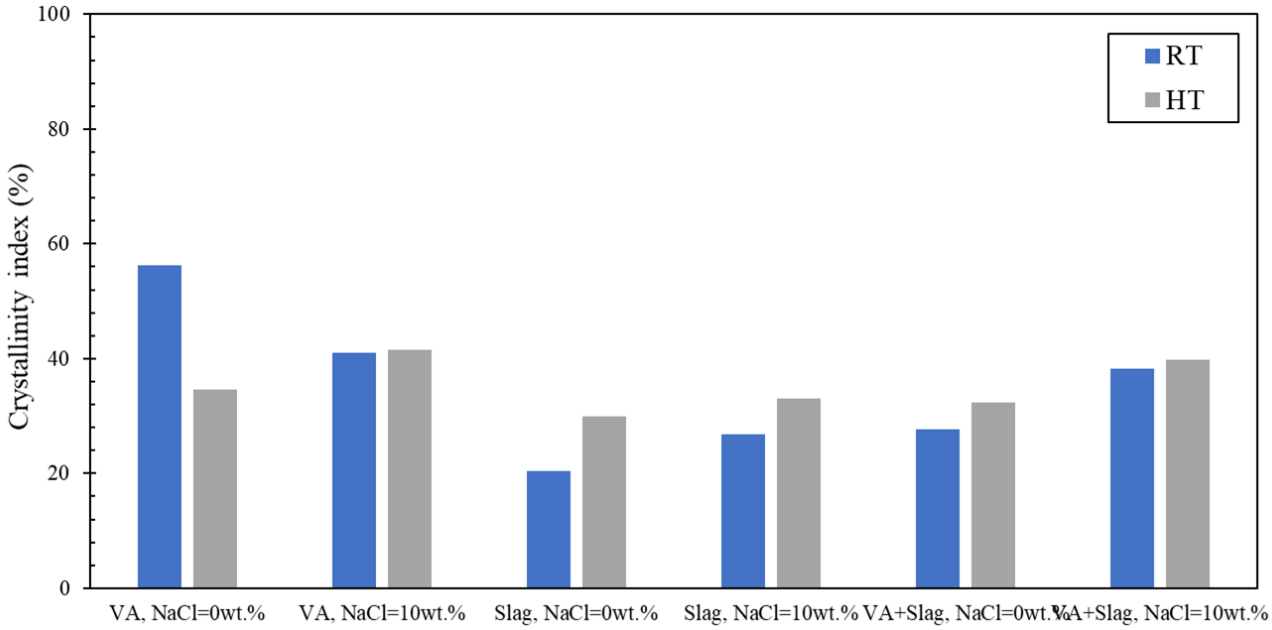


Fig. 8. Crystallinity index (CI) of the alkali activated (100 wt.% VA), alkali activated (100 wt.% slag), and alkali activated (50 wt.% VA+50 wt.% slag) in HT and RT conditions.

### 3.2.2. FTIR analysis

FTIR spectroscopy has been performed to further investigate changes in amorphous bonds. This analysis shows the chemical structure of the bonds based on the amount of vibration made by the bond, Table 4.

Table 4. Characteristic FTIR bands of the alkali activated cements.

| Wave number ($cm^{-1}$) | Assignment |
|---|---|
| 450-490 | Asymmetric bending vibration (Si-O-Si and Si-O-Al) |
| 550-750 | Symmetric bending vibration (Si-O-T (Si or Al)) |
| 770-800 | Symmetric stretching vibration (Si-O-Si) |
| 860-890 | Stretching vibration (Al-O, Si-O) |
| 900-1100 | Asymmetric stretching vibration (Si-O-T (Si or Al)) |
| 1410-1440 | Stretching vibration (O-C-O) |
| 1600-1700 | Bending vibration (H-O-H, -OH) |
| 2300-2400 | Stretching vibration (H-O-H, -OH) |
| 3000-3500 | Stretching vibration (H-O-H, -OH) |

Fig. 9 shows the FTIR spectra of alkali activated cement pastes in both RT and HT conditions.

In general, the bands observed in the range of 450-1100 $cm^{-1}$ were related to aluminosilicate bonds in phases N-A-S-H and C-A-S-H.

The lower the wave number and the deeper the peak, the higher the density of the bond. In all alkali activated specimens and in both curing conditions, the presence of sodium chloride led to a deeper wave peak and a reduction in wave number in the range of 450-1100 $cm^{-1}$ compared to the samples without sodium chloride. This can indicate higher density of N-A-S-H and C-A-S-H gels, resulting in a higher density of the geopolymer structure and ultimately increased mechanical strength of the samples. It can also be concluded that the addition of sodium chloride changed the chemical structure of geopolymer cements and strengthened the hypothesis of sodium chloride encapsulation by the geopolymer structure observed in the XRD results.

In RT curing condition, the waves observed in the range of 450-1100 $cm^{-1}$, which are related to aluminosilicate bonds, were more intense in samples containing slag (50 and 100 wt.% slag) [72-74]. However, in HT curing condition, these peaks were more intense in samples containing volcanic ash (without slag). Also, from comparing Figs. 9b and 9c with Fig. 9a, it can be seen that as the amount of slag in the samples increased, the intensity of the waves increased dramatically in the range of 450-1100 $cm^{-1}$ (deeper peaks), which indicated N-A-S-H and C-A-S-H gels were denser and improved the mechanical strength of samples, which was consistent with XRD results.

The bands in the range 550-750 $cm^{-1}$ indicated the presence of an amorphous aluminosilicate structure in all samples [75].

The bands in the range of 1600-1700 $cm^{-1}$ were related to crystalline water, and the bands in the range of 2300-2400 $cm^{-1}$ and 3000-3500 $cm^{-1}$ were related to physical water [72-74]. These water molecules were present on the surface or inside the geopolymer cavities. The bands observed in

the range of 1600-1700 $cm^{-1}$, as well as in the range of 2300-2400 $cm^{-1}$ and 3000-3500 $cm^{-1}$, were significantly intensified by alkaline activation of aluminosilicate precursors. This was true for both volcanic ash and slag samples. This indicated more water uptake by the geopolymer structure and possibly the presence of water-hydrated compounds in the system [76]. On the other hand, for the samples containing sodium chloride, the intensity of these peaks was higher, which could be due to the better formation of geopolymer gel in these samples, which had an effect on the mechanical results and prevented the mechanical strength reduction due to the addition of sodium chloride. In other words, the presence of a stronger O-H bond means higher water absorption and ultimately higher alkaline conditions in the environment, due to which a higher pH is created in the environment. In this line, the hydration of the products was well done, which increased the mechanical properties. Previous research has shown that the O-H bond formed between 3000-3500 $cm^{-1}$ can be related to the C-S-H bond, which indicated that the stronger the peak, the stronger the bond [72-74]. Comparing Figs. 9b and 9c with Fig. 9a, it can be seen that by increasing the amount of slag, the peaks formed in the range of 1600-1700 $cm^{-1}$ and also in the range of 2300-2400 $cm^{-1}$ and 3000-3500 $cm^{-1}$ have deepened and this has led to improved mechanical strength compared to samples without slag.

The bands observed in the range of 1410-1440 $cm^{-1}$ were related to the carbonates formed due to the reaction of alkaline metal hydroxides in the geopolymer with $CO_2$ in the air [72-74]. As the amount of slag and the amount of sodium chloride increased, the amount of bond formed increased. In ambient temperature curing condition, since the specimens were in direct contact with air, the amount of carbonate bond formation was higher between 1410-1440 $cm^{-1}$. Therefore, in ambient temperature curing condition, the intensity of this peak was higher than corresponding samples in hydrothermal curing condition.

The bands in the range of 860-890 $cm^{-1}$ were related to the Al-O or Si-O bond [72, 73]. This bond was more clearly visible in samples containing slag and the reason for the increase in strength in samples containing 50 and 100 wt.% slag can be due to this bond. The peak of Al-O or Si-O bonding in the range of 860-890 $cm^{-1}$ in hydrothermal curing condition was more severe than the ambient temperature curing condition.

In ambient temperature curing condition, the peaks formed due to hydroxyl bonds (O-H) were more intense in samples containing slag (50 and 100 wt.% slag) (Figs. 9b and 9c). While these peaks were more intense in samples containing volcanic ash (without slag) in HT curing condition. Therefore, hydrothermal curing condition was more suitable for samples containing volcanic ash consistent with XRD results. Because in hydrothermal conditions, both water and temperature factors that were suitable for the formation of geopolymer structure were present at the same time, and this issue strengthened the geopolymer structure and the formation of hydroxyl bonds (O-H).

a)

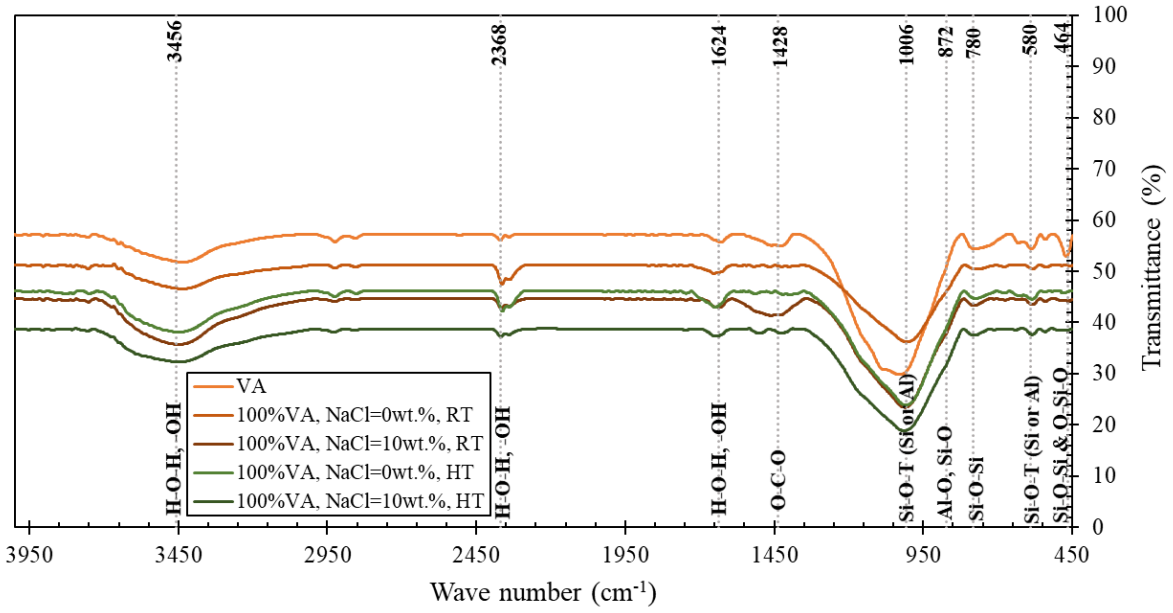

504 b)

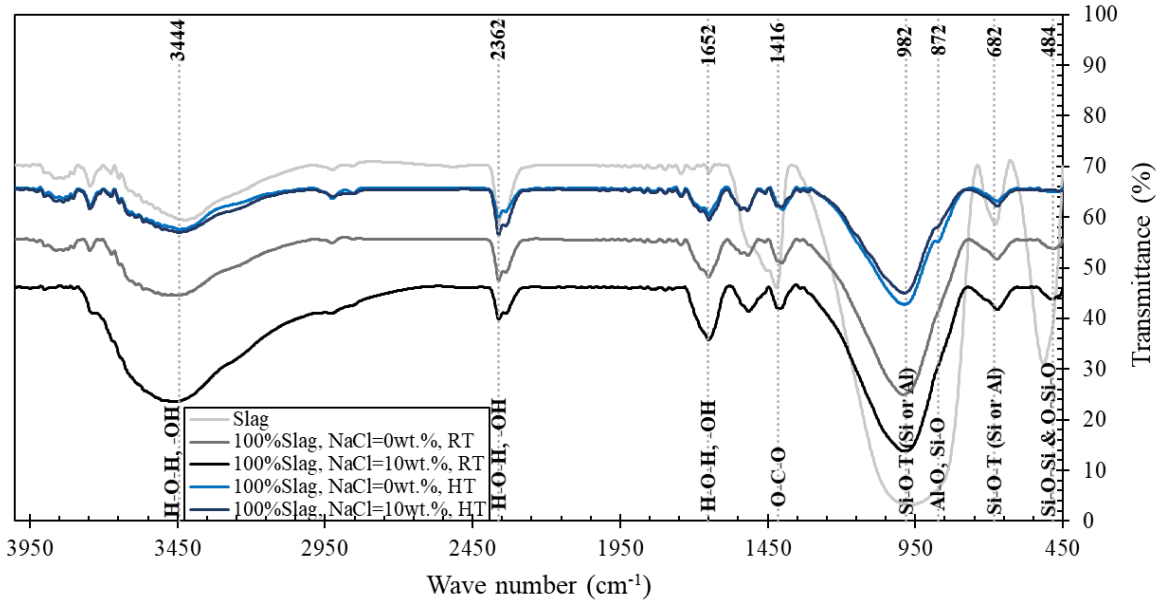


505

506

507

508

509

510

511 c)

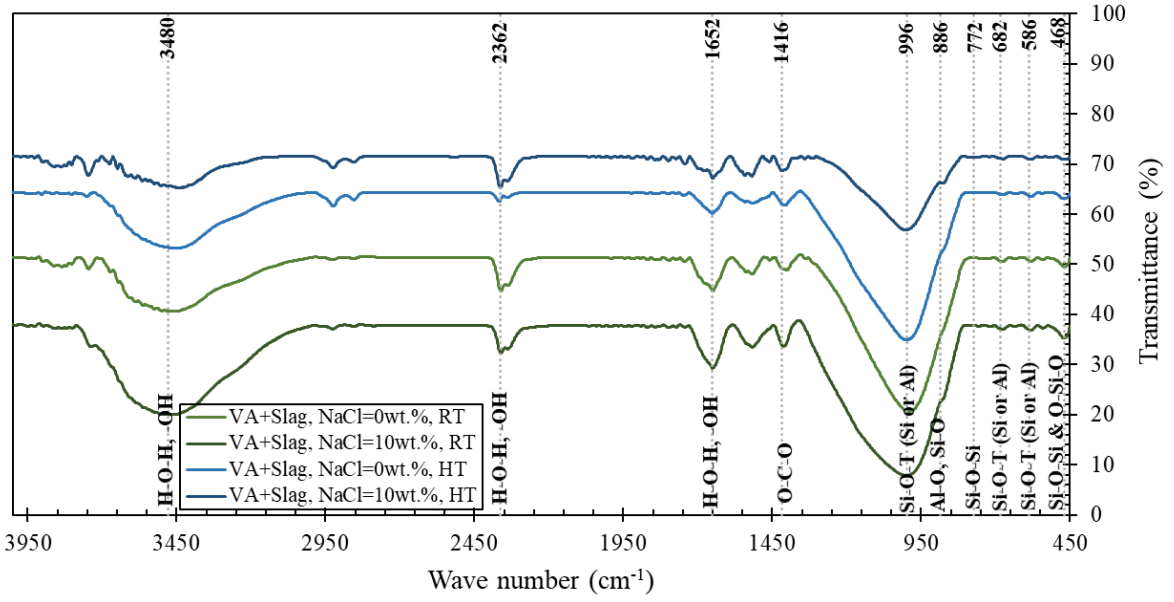


512

Fig. 9. FTIR spectra of the a) alkali activated (100 wt.% VA), b) alkali activated (100 wt.% slag) c) alkali activated (50 wt.% VA+50 wt.% slag), in HT and RT conditions.

### 3.2.3. SEM-EDS-Mapping analysis

Scanning electron microscopy (SEM) images have been used to examine changes in the structure of the geopolymer matrix.

In Fig. 10, the microstructure of VA-based samples in HT curing condition had a denser structure than ambient temperature condition, and also samples containing sodium chloride had a denser structure than samples without sodium chloride. In samples containing 50 and 100 wt.% slag (Figs. 11 and 12), the addition of sodium chloride in both curing conditions resulted in structural cracks, possibly due to the formation of Friedel's salt. The results of previous studies have shown that the presence of slag can reduce the diffusion rate of chloride ions and increase the formation of Friedel's salt [8, 28]. Also, due to the increase in volume due to the formation of Friedel's salt, large cracks were formed in the samples, which led to a decrease in mechanical strength in high amounts of sodium chloride [8].

Comparing the Figs. 11 and 12, more microcracks were observed in the alkali activated samples containing 50 wt.% VA and 50 wt.% slag than slag-based samples. These microcracks might be formed as a result of the formation of two or more types of gels in the microstructure, which are not integrated together, therefore, the compact microstructure cannot form. Thus, samples containing 100 wt.% slag showed higher compressive strength than samples containing 50 wt.% slag.

As observed in the XRD results, the addition of slag to the samples led to an increase in the amorphous phase and a decrease in the crystalline phase, which has been observed in previous

studies [14]. This has caused the compressive strength of the samples to increase with increasing slag percentage. In SEM images, the change in morphology of the gels formed in the samples containing slag (Figs. 11 and 12) compared to the samples without slag (Fig. 10) is clearly visible. Numerous flakes were arranged into solid structures in VA-based alkali activated samples, Fig. 10. While, a small number of granular bodies that came into contact with each other were suspended in a lamellar matrix, Figs. 11 and 12. It can be attributed to a large amount of silicate hydration products such as C-S-H, N-(C)-A-S-H and C-A-S-H formed by the hydration reaction of slag.

Comparing the Figs. 10-12, the amount of slag hydration products increased with increased slag content. These products filled the pores and caused the cementitious matrix to become denser which led to a mechanical strength development in slag-based alkali activated samples. Previous studies have shown that the formation of C-S-H gel due to hydration of slag leads to reduced porosity and consequently a denser structure and ultimately reduced chloride ion mobility in slag concretes [30-32].

When volcanic ash was activated, the predominant gel was N-A-S-H, the most well-known type of geopolymer gel. When the slag replaced 50 wt.% of the volcanic ash, the gel type moved to a gel with a small amount of calcium, N-(C)-A-S-H. In other words, some sodium ions were replaced by calcium ions. In a similar study performed by combining 75 wt.% fly ash with 25 wt.% slag, the occurrence of this gel was confirmed [22]. Finally, when the slag completely replaced the volcanic ash, the predominant gel was C-A-S-H.

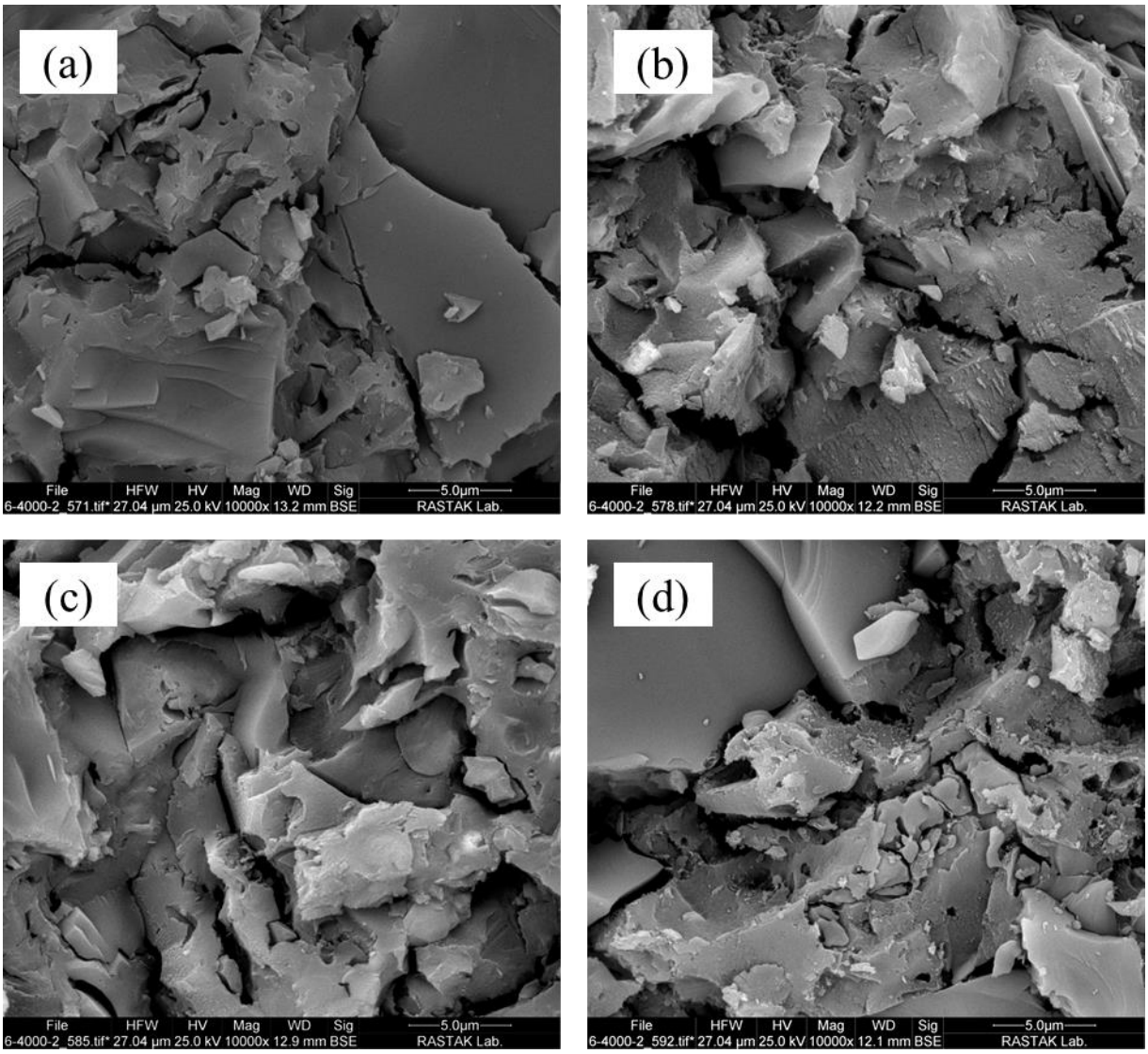


Fig. 10. The SEM images of the VA-based alkali activated samples in RT condition (90 days curing), a) without NaCl, b) with 10 wt.% NaCl and HT condition, c) without NaCl, d) with 10 wt.% NaCl.

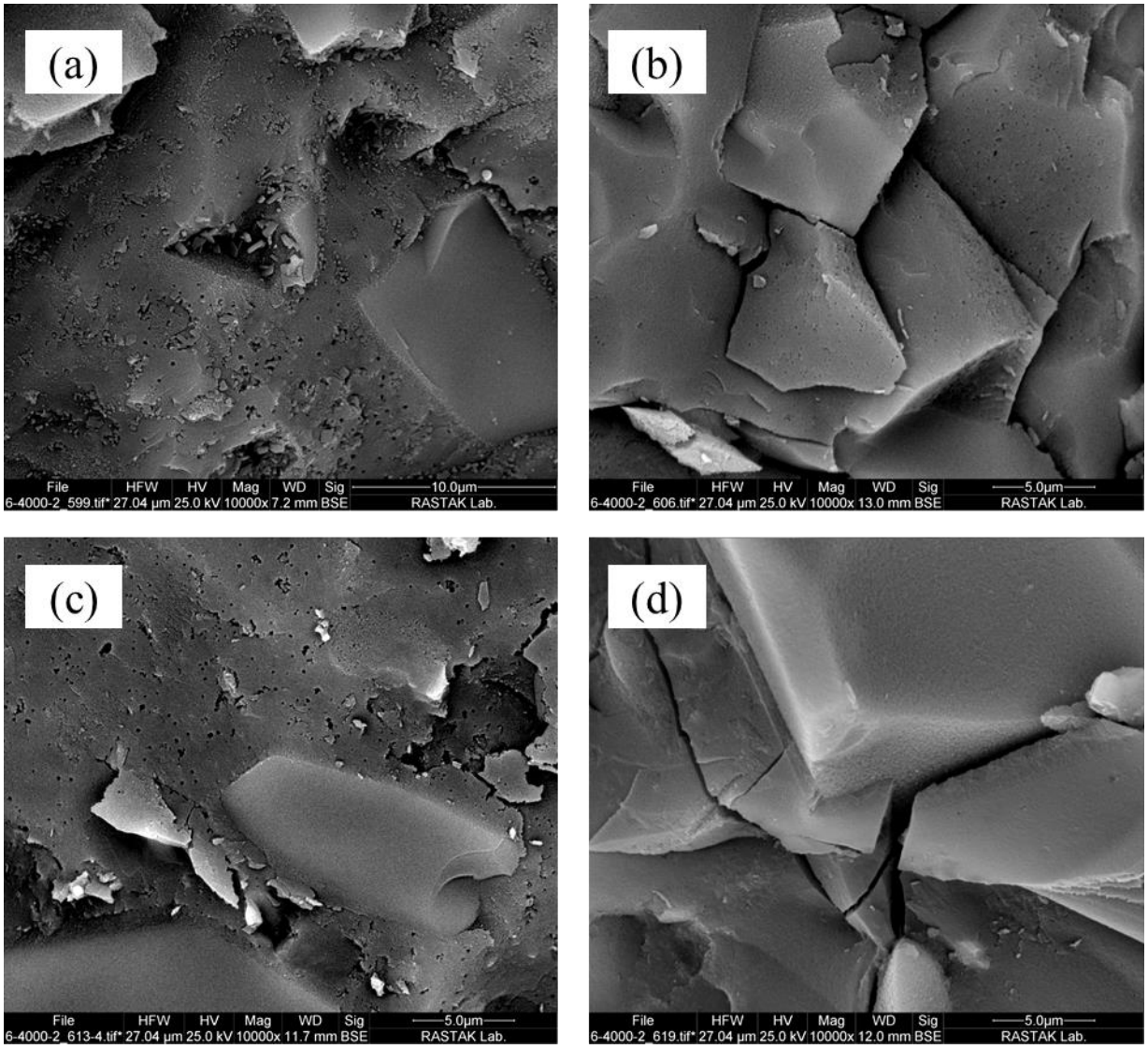


Fig. 11. The SEM images of the Slag-based alkali activated samples in RT condition (90 days curing), a) without NaCl, b) with 10 wt.% NaCl and HT condition, c) without NaCl, d) with 10 wt.% NaCl.

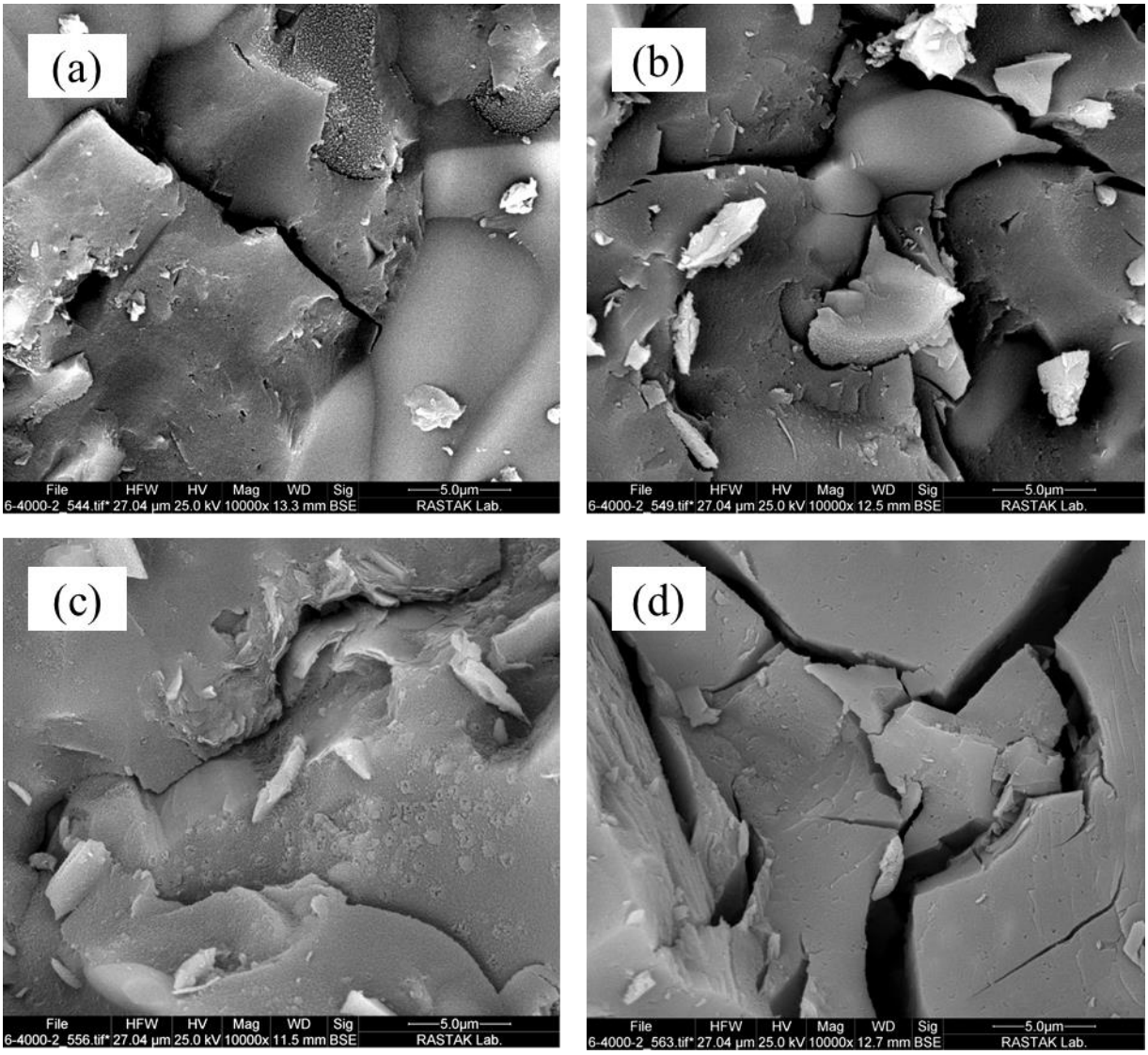


Fig. 12. The SEM images of the alkali activated samples cotaining 50 wt.% VA and 50 wt.% slag in RT condition (90 days curing), a) without NaCl, b) with 10 wt.% NaCl and HT condition, c) without NaCl, d) with 10 wt.% NaCl.

From the EDS results, Figs. 13-15, it can be seen that at points where the elemental analysis values were close to the aluminosilicate precursors, the reaction did not occur well. These particles remained unreacted (Figs. b, d, f and h) resulting in a reduction in mechanical strength. Also, the porosity created in the sample due to the rapid evaporation of water from the sample led to a decrease in the strength of the samples. In general, the presence of calcium, aluminum, silicon and

sodium indicated the formation of N-A-S-H gel, C-A-S-H gel and also (N, C)-A-S-H gel. The presence of large amounts of sodium and calcium indicated the formation of more of these gels. The high Si/Ca ratio in VA-based alkali activated samples indicated the predominance of N-A-S-H gel, which is consistent with XRD results. As the amount of slag increased, C-S-H and C-A-S-H gels prevailed and the Si/Ca ratio decreased. The simultaneous formation of these two gels caused the structure to thicken and thus increased the strength in the samples containing slag, which is completely consistent with the results of XRD and FTIR analysis.

Theoretically, C-A-S-H gel had a positively charged surface in alkaline environments, and the higher the positive charge, the greater the ability to absorb $OH^-$ ions and chloride ions [27]. The higher the Si/Ca ratio, the lower the adsorption capacity of this gel as the positive charge of this gel decreased.

The higher the Cl/Al ratio in the EDS of the reactive zone (geopolymer gel), the more chloride ions were encapsulated in the gel and the solidification process has taken place. In samples containing sodium chloride, the amount of chloride in elemental analysis increased significantly, especially in the reactive sections, which is consistent with the results of XRD analysis and FTIR analysis. With the obtained results, the hypothesis of physical adsorption of chloride ion on geopolymer gels as well as the hypothesis of chloride ion encapsulation in geopolymer matrix are strengthened.

600

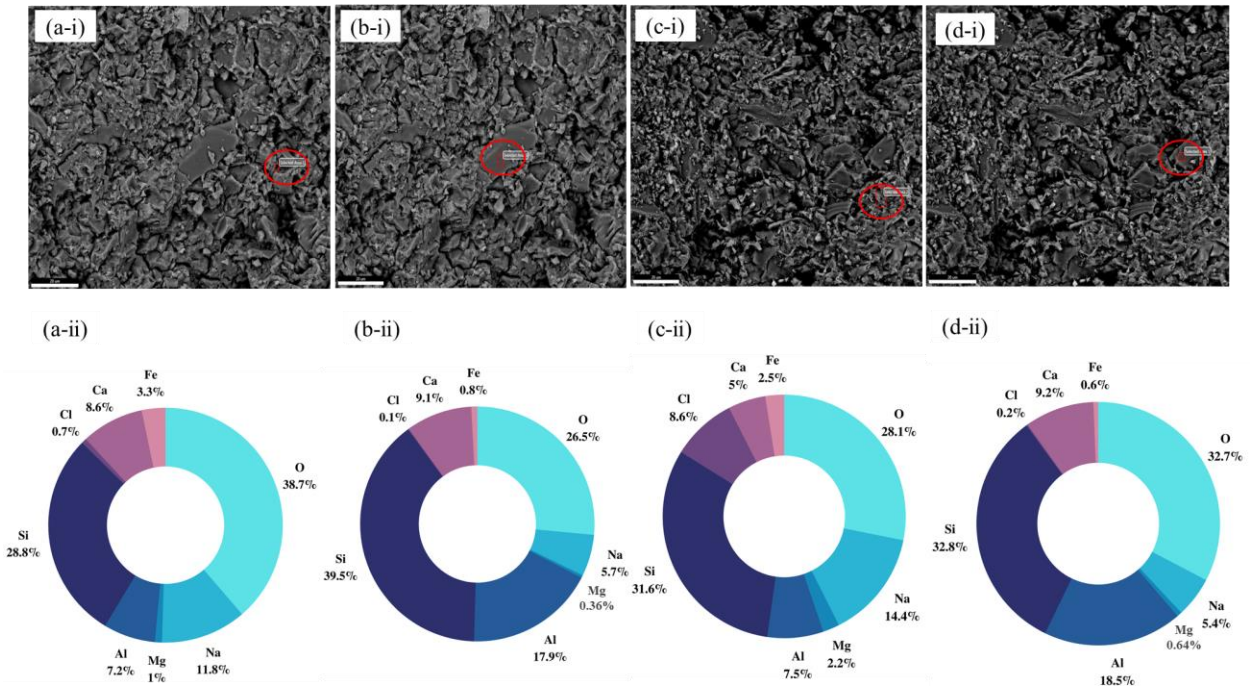


601

602

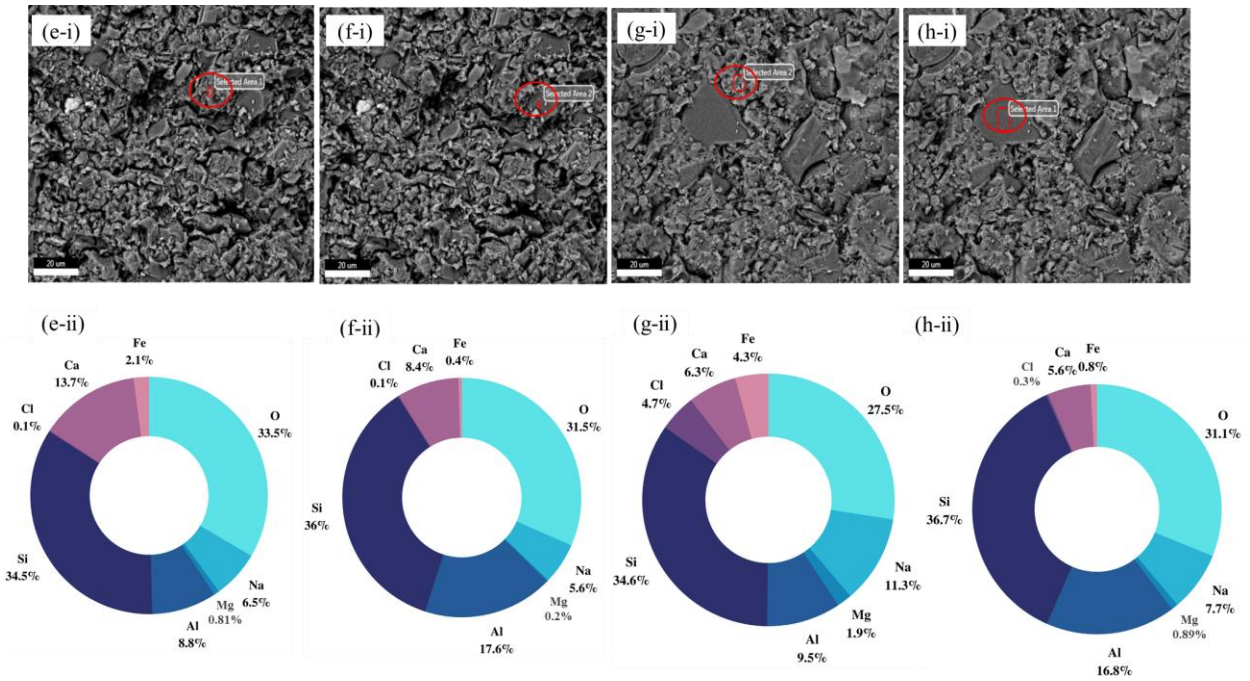


603

| Parameter | Region | | | | | | | |
|---|---|---|---|---|---|---|---|---|
| | a | b | c | d | e | f | g | h |
| Si/Ca | 3.35 | 4.34 | 6.32 | 3.57 | 2.52 | 4.29 | 5.49 | 6.55 |
| Cl/Al | 0.1 | 0.006 | 1.15 | 0.010 | 0.011 | 0.006 | 0.49 | 0.018 |

Fig. 13. EDS analysis of the VA-based alkali activated samples in RT condition (90 days curing), a,b) without NaCl, c,d) with 10 wt.% NaCl and HT condition, e,f) without NaCl, g,h) with 10 wt.% NaCl.

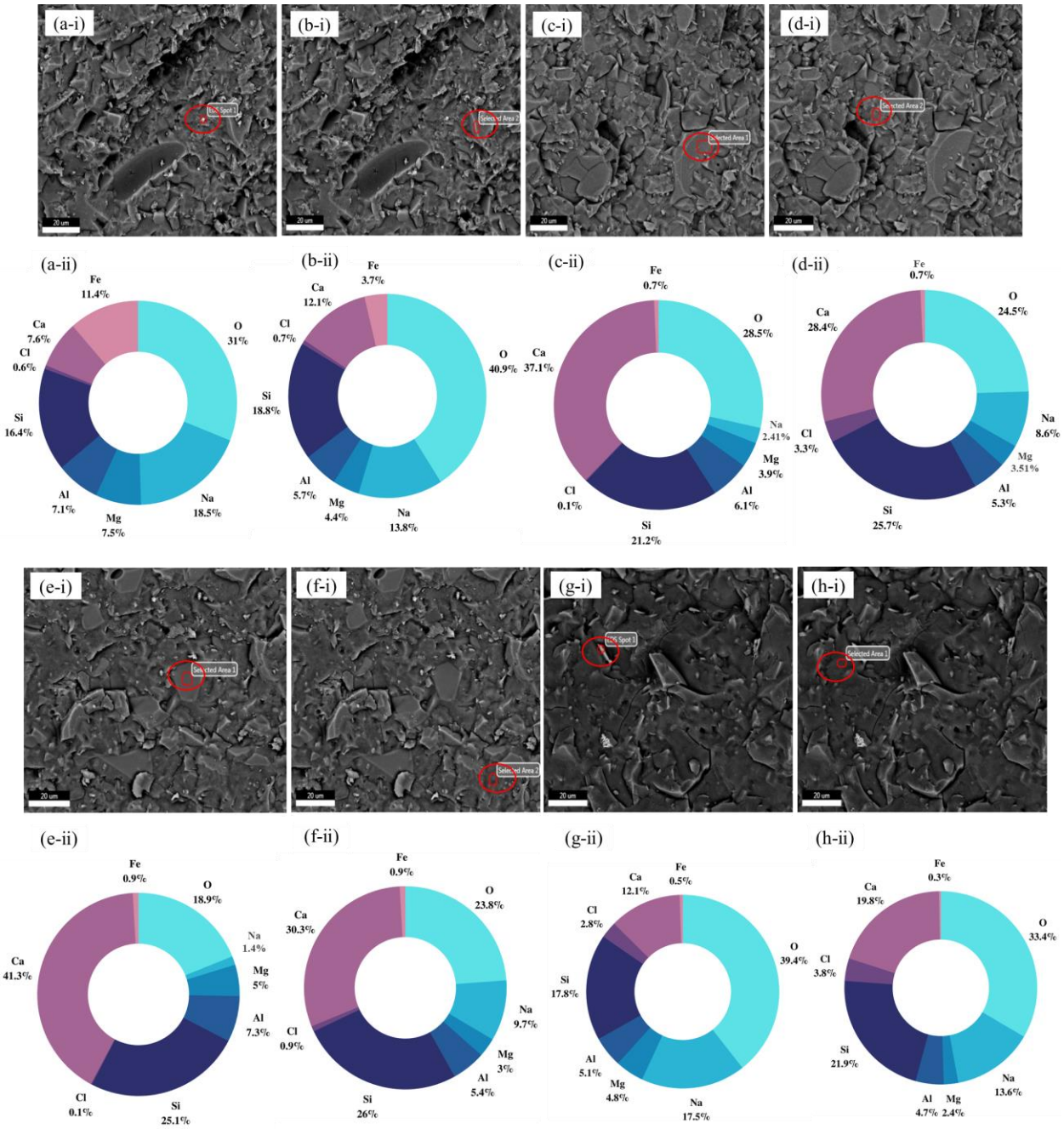


| Parameter | Region | | | | | | | |
|---|---|---|---|---|---|---|---|---|
| | a | b | c | d | e | f | g | h |

| | | | | | | | | |
|---|---|---|---|---|---|---|---|---|
| Si/Ca | 2.16 | 1.55 | 0.57 | 0.90 | 0.61 | 0.86 | 1.47 | 1.11 |
| Cl/Al | 0.085 | 0.12 | 0.016 | 0.62 | 0.014 | 0.17 | 0.55 | 0.81 |

611

612 Fig. 14. EDS analysis of the slag-based alkali activated samples in RT condition (90 days
613 curing), a,b) without NaCl, c,d) with 10 wt.% NaCl and HT condition, e,f) without NaCl, g,h)
614 with 10 wt.% NaCl.

615

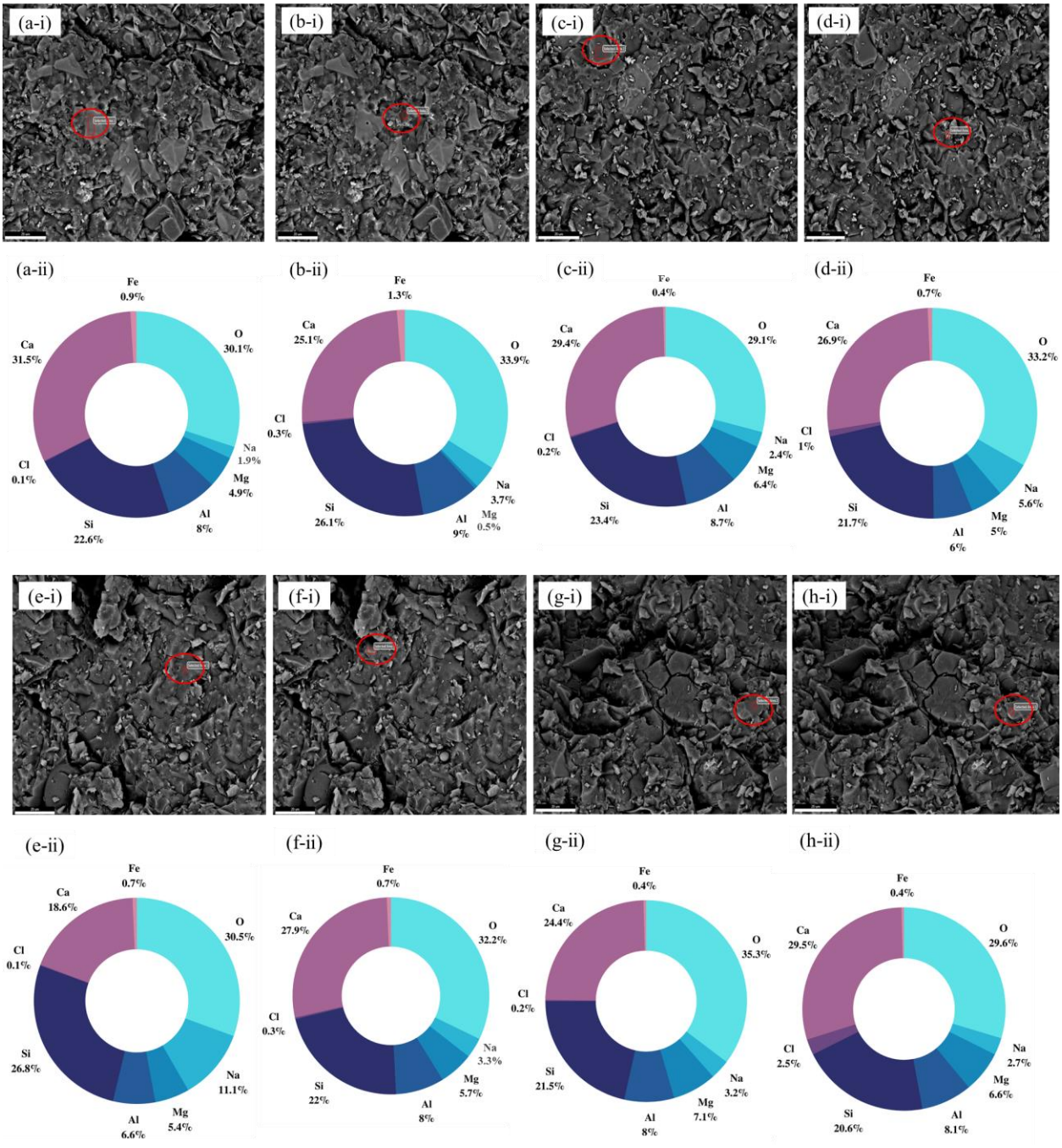


616

617

| Parameter | Region | | | | | | | |
|---|---|---|---|---|---|---|---|---|
| | a | b | c | d | e | f | g | h |
| Si/Ca | 0.72 | 1.03 | 0.79 | 0.81 | 1.44 | 0.79 | 0.88 | 0.7 |
| Cl/Al | 0.013 | 0.033 | 0.023 | 0.17 | 0.015 | 0.038 | 0.025 | 0.31 |

Fig. 15. EDS analysis of the alkali activated samples cotaining 50 wt.% VA and 50 wt.% slag in RT condition (90 days curing), a,b) without NaCl, c,d) with 10 wt.% NaCl and HT condition, e,f) without NaCl, g,h) with 10 wt.% NaCl.

According to Figs. 16 and 17, the appropriate formation of N-A-S-H gel in the structure of VA-based alkali activated samples was linked to a generally uniform distribution of sodium, aluminum, and silicon elements. In slag-based samples, the concentration of calcium increased significantly, indicating the formation of C-S-H gels as well as C-A-S-H gels.

In samples containing sodium chloride, the chloride ion density increased significantly and its relatively uniform dispersion indicated its adsorption by geopolymer gels, complying with the XRD and FTIR results.

a)

641

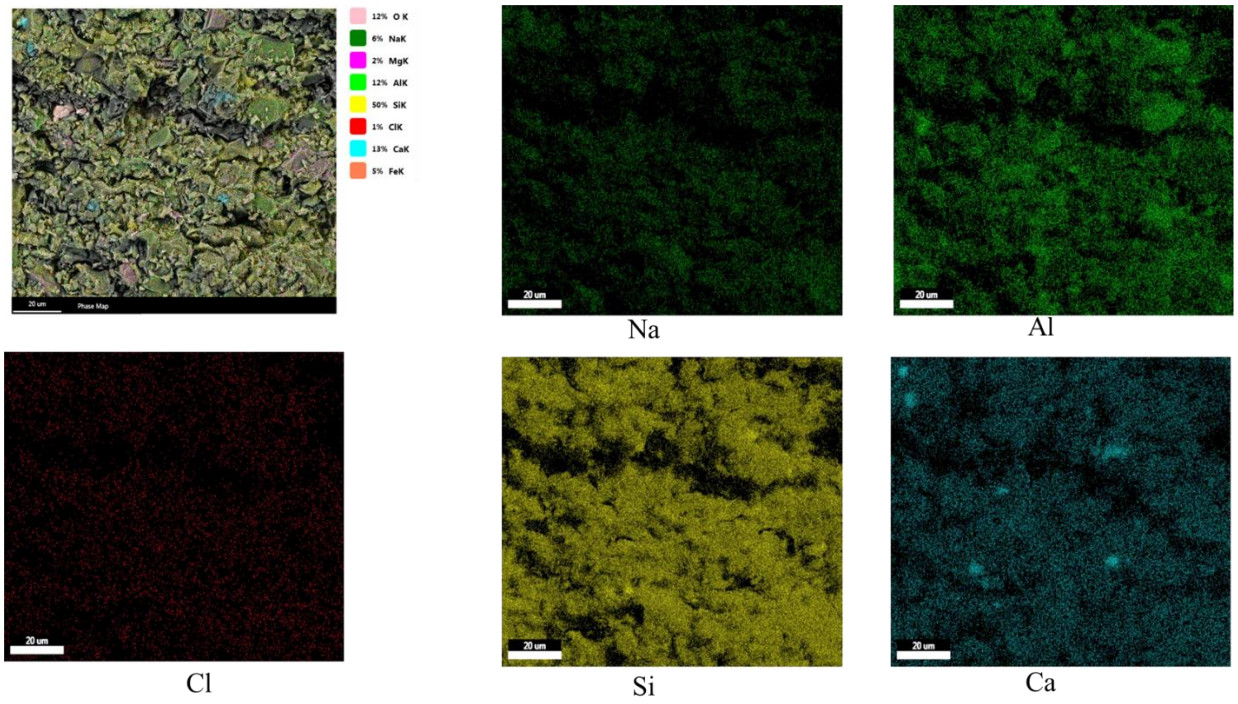


642

643 b)

644

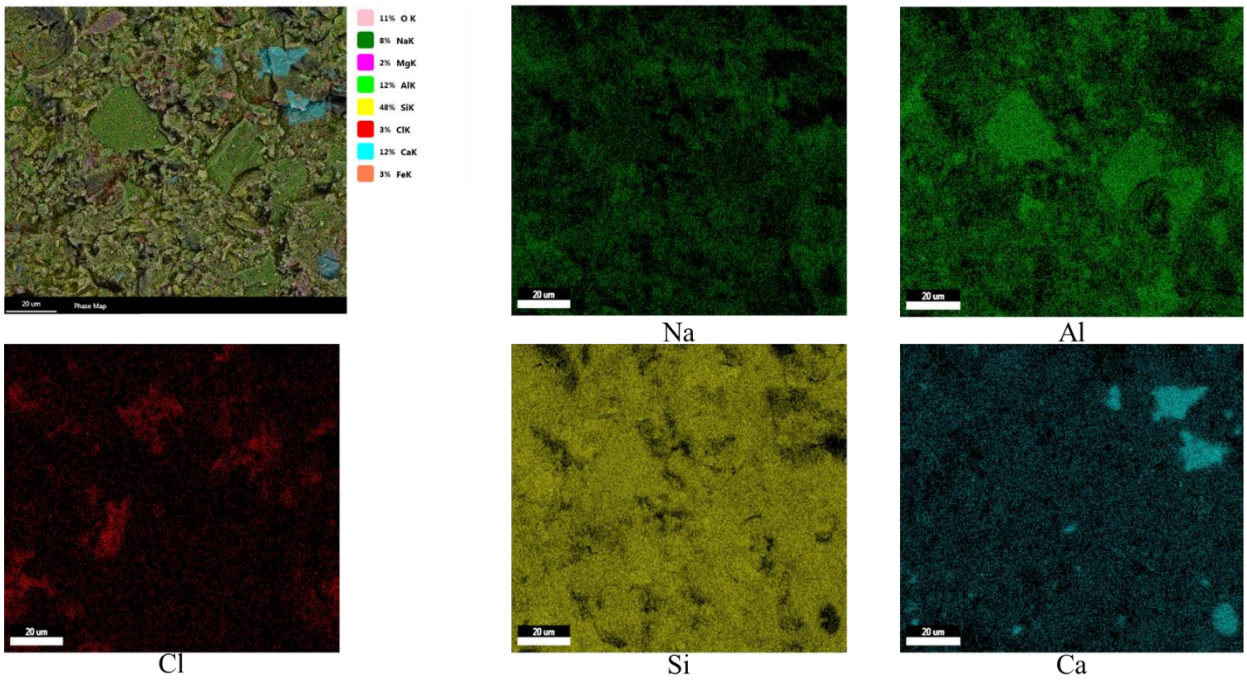


645

646

Fig. 16. Elemental Mapping analysis of the VA-based alkali activated samples in HT condition, a) without NaCl, b) with 10 wt.% NaCl.

a)

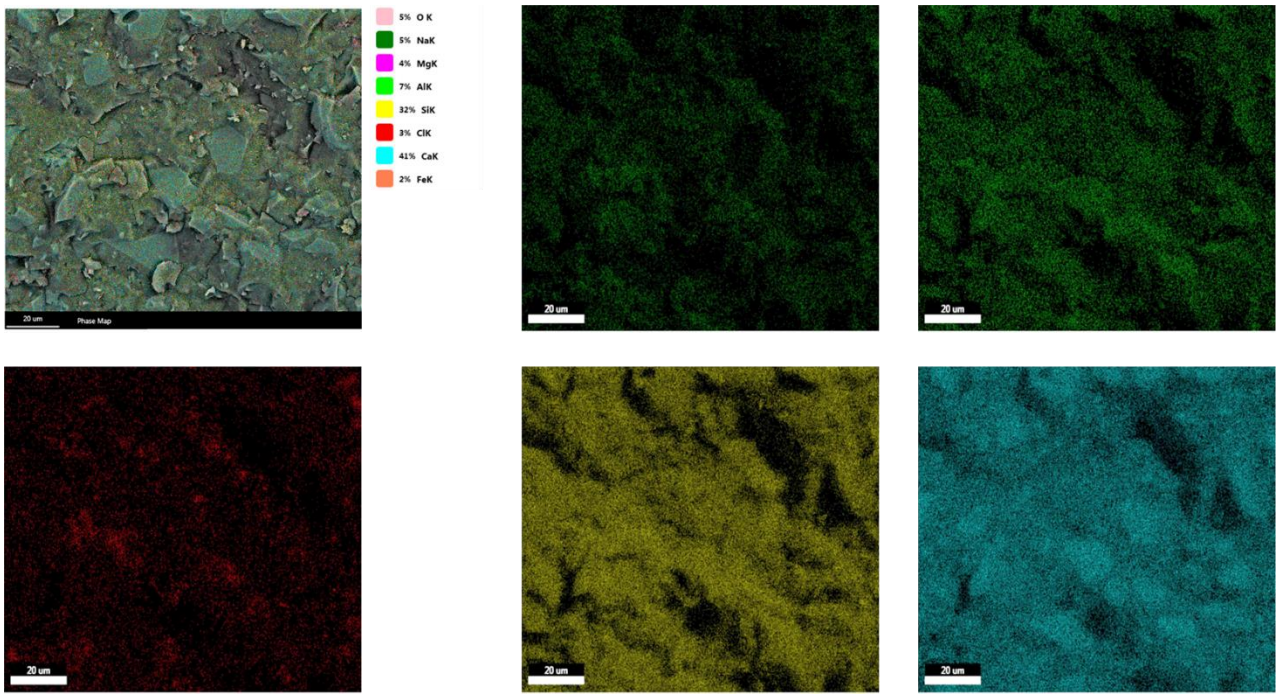


b)

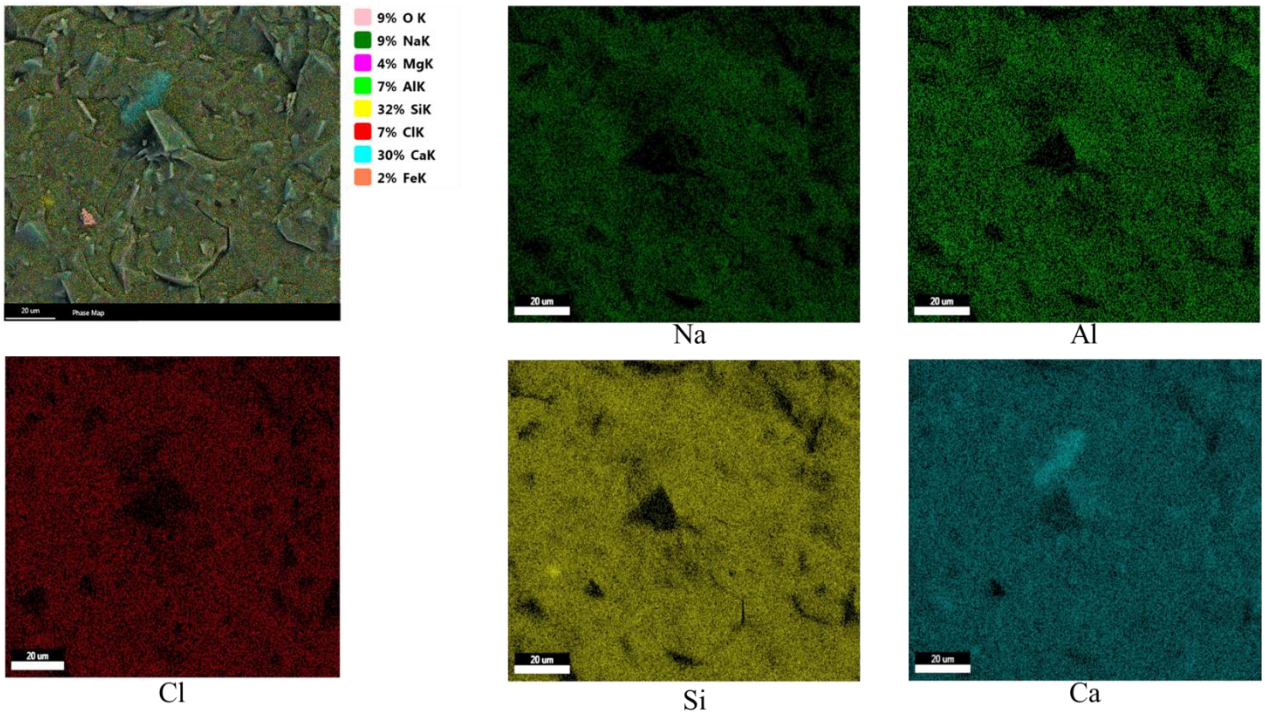

Fig. 17. Elemental Mapping analysis of the slag-based alkali activated samples in HT condition, a) without NaCl, b) with 10 wt.% NaCl.

## 4. Conclusions

Generally, samples containing 100 wt.% slag showed the highest compressive strength, followed by samples containing 50 wt.% slag, Portland cement, and 100 wt.% volcanic ash in both curing conditions.

The addition of sodium chloride from 0 to 10 wt.% did not significantly affect the strength of samples containing 100 wt.% volcanic ash in both HT and RT conditions. However, in HT condition, the mechanical strength of samples containing 50 and 100 wt.% slag as well as Portland cement pastes increased with increasing sodium chloride from 0 to 2.5 wt.%, and further addition of sodium chloride by up to 10 wt.% led to mechanical strength reduction. On the other side, in RT condition, the strength of samples containing 50 and 100 wt.% slag as well as Portland cement samples decreased with the addition of sodium chloride from 0 to 10 wt.%.

N-A-S-H gel in VA-based samples and (N,C)-A-S-H and C-S-H gels in slag-based samples were the main factor in strength development of alkali activated cement pastes. In VA-based samples, N-A-S-H gel became more intense as the amount of sodium chloride increased. Meanwhile, the solidification and encapsulation of chloride ions in the dense structure of slag-based samples was the predominant mechanism in chloride adsorption.

Addition of slag in the precursor led to the higher mechanical strength of alkali activated cement than Portland cement against the addition of chloride ions in both curing conditions. Besides, high content of CaO in slag played a significant role in Ca-Al-LDH formation that resulted in Friedel's salt.

In Portland cement pastes, the chemical adsorption of chloride ions depends on Friedel's salt. Meanwhile, the adsorption mechanism of chloride ions in alkali activated slag includes physical adsorption by C-S-H gel and chemical adsorption by Cl-hydrocalumite and Cl-hydrotalcite.

## CRediT authorship contribution statement

**Pooria Ghadir:** Conceptualization, Data curation, Formal analysis, Writing – original draft, Investigation, Visualization, Methodology. **Hamid Reza Razeghi:** Writing - review & editing, Validation, Resources.

## Declaration of Competing Interest

The authors declare no conflict of interest.

## Acknowledgment

The authors would like to acknowledge Iran's National Elites Foundation. Also, we would like to appreciate the efforts of Professor Nader Shariatmadari and Ms. Parisa Samadi. This study was supported by Chem Concrete Pty Ltd (No. 120/3F1400) and MatSoil company (No. 01A/2022).

## References

1. Chen, Z. and H. Ye, *Influence of metakaolin and limestone on chloride binding of slag activated by mixed magnesium oxide and sodium hydroxide.* Cement and Concrete Composites, 2021: p. 104397.
2. Kohail, M. and M.A. Khalaf, *The efficiency of chloride extraction using un-galvanized steel anode.* Ain Shams Engineering Journal, 2021. **12**(2): p. 1353-1360.
3. Hirao, H., et al., *Chloride binding of cement estimated by binding isotherms of hydrates.* Journal of Advanced Concrete Technology, 2005. **3**(1): p. 77-84.
4. Birnin-Yauri, U. and F. Glasser, *Friedel's salt, Ca2Al (OH) 6 (Cl, OH)· 2H2O: its solid solutions and their role in chloride binding.* Cement and Concrete Research, 1998. **28**(12): p. 1713-1723.
5. Thomas, M., et al., *The effect of supplementary cementitious materials on chloride binding in hardened cement paste.* Cement and Concrete Research, 2012. **42**(1): p. 1-7.
6. Yoon, S., et al., *Phase changes of monosulfoaluminate in NaCl aqueous solution.* Materials, 2016. **9**(5): p. 401.
7. De Weerdt, K., D. Orsáková, and M.R. Geiker, *The impact of sulphate and magnesium on chloride binding in Portland cement paste.* Cement and Concrete Research, 2014. **65**: p. 30-40.
8. He, W., C. Liu, and L. Zhang, *Effects of sodium chloride on the mechanical properties of slag composite matrix geopolymer.* Advances in Cement Research, 2019. **31**(9): p. 389-398.
9. Li, P., et al., *Investigation on early-age hydration, mechanical properties and microstructure of seawater sea sand cement mortar.* Construction and Building Materials, 2020. **249**: p. 118776.

10. Farnam, Y., et al., *The influence of calcium chloride deicing salt on phase changes and damage development in cementitious materials.* Cement and Concrete Composites, 2015. **64**: p. 1-15.
11. Rocha, C.A.A., G.C. Cordeiro, and R.D. Toledo Filho, *Use of thermal analysis to determine the hydration products of oil well cement pastes containing NaCl and KCl.* Journal of Thermal Analysis and Calorimetry, 2015. **122**(3): p. 1279-1288.
12. Brough, A., et al., *Sodium silicate-based alkali-activated slag mortars: Part II. The retarding effect of additions of sodium chloride or malic acid.* Cement and Concrete Research, 2000. **30**(9): p. 1375-1379.
13. Shariatmadari, N., et al., *Compressive strength of sandy soils stabilized with alkali-activated volcanic ash and slag.* Journal of Materials in Civil Engineering, 2021. **33**(11): p. 04021295.
14. Miraki, H., et al., *Clayey soil stabilization using alkali-activated volcanic ash and slag.* Journal of Rock Mechanics and Geotechnical Engineering, 2021.
15. Mohammadifar, L., et al., *Properties of Lime-Cement Concrete Containing Various Amounts of Waste Tire Powder under Different Ground Moisture Conditions.* Polymers, 2022. **14**(3): p. 482.
16. Ghadir, P., et al., *Shear strength and life cycle assessment of volcanic ash-based geopolymer and cement stabilized soil: A comparative study.* Transportation Geotechnics, 2021. **31**: p. 100639.
17. Ghadir, P. and N. Ranjbar, *Clayey soil stabilization using geopolymer and Portland cement.* Construction and Building Materials, 2018. **188**: p. 361-371.
18. Gunasekara, C., et al., *Chloride induced corrosion in different fly ash based geopolymer concretes.* Construction and Building Materials, 2019. **200**: p. 502-513.
19. Ke, X., S.A. Bernal, and J.L. Provis. *Chloride binding capacity of synthetic C–(A)–S–H type gels in alkali-activated slag simulated pore solutions*. in *Proceedings of the 1st international conference on construction materials for sustainable future, Zadar, Croatia*. 2017.
20. Mayhoub, O.A., et al., *Effect of curing regimes on chloride binding capacity of geopolymer.* Ain Shams Engineering Journal, 2021.
21. Dhir, R., M. El-Mohr, and T. Dyer, *Developing chloride resisting concrete using PFA.* Cement and Concrete Research, 1997. **27**(11): p. 1633-1639.
22. Ismail, I., et al., *Influence of fly ash on the water and chloride permeability of alkali-activated slag mortars and concretes.* Construction and Building Materials, 2013. **48**: p. 1187-1201.
23. Babaee, M. and A. Castel, *Chloride diffusivity, chloride threshold, and corrosion initiation in reinforced alkali-activated mortars: Role of calcium, alkali, and silicate content.* Cement and Concrete Research, 2018. **111**: p. 56-71.
24. Ke, X., et al., *Chloride binding and mobility in sodium carbonate-activated slag pastes and mortars.* Materials and structures, 2017. **50**(6): p. 1-13.
25. Li, C., et al., *Pozzolanic reaction of fly ash modified by fluidized bed reactor-vapor deposition.* Cement and Concrete Research, 2017. **92**: p. 98-109.
26. Siddique, S. and J.G. Jang, *Mechanical Properties, Microstructure, and Chloride Content of Alkali-Activated Fly Ash Paste Made with Sea Water.* Materials, 2020. **13**(6): p. 1467.
27. Zhang, J., C. Shi, and Z. Zhang, *Chloride binding of alkali-activated slag/fly ash cements.* Construction and Building Materials, 2019. **226**: p. 21-31.
28. Roy, D.M., W. Jiang, and M. Silsbee, *Chloride diffusion in ordinary, blended, and alkali-activated cement pastes and its relation to other properties.* Cement and Concrete research, 2000. **30**(12): p. 1879-1884.
29. Ye, H., L. Huang, and Z. Chen, *Influence of activator composition on the chloride binding capacity of alkali-activated slag.* Cement and Concrete Composites, 2019. **104**: p. 103368.
30. Khan, M., O. Kayali, and U. Troitzsch, *Chloride binding capacity of hydrotalcite and the competition with carbonates in ground granulated blast furnace slag concrete.* Materials and Structures, 2016. **49**(11): p. 4609-4619.
31. Song, H.-W. and V. Saraswathy, *Studies on the corrosion resistance of reinforced steel in concrete with ground granulated blast-furnace slag—An overview.* Journal of Hazardous materials, 2006. **138**(2): p. 226-233.

32. Leng, F., N. Feng, and X. Lu, *An experimental study on the properties of resistance to diffusion of chloride ions of fly ash and blast furnace slag concrete.* Cement and Concrete Research, 2000. **30**(6): p. 989-992.
33. Kayali, O., M. Khan, and M.S. Ahmed, *The role of hydrotalcite in chloride binding and corrosion protection in concretes with ground granulated blast furnace slag.* Cement and Concrete Composites, 2012. **34**(8): p. 936-945.
34. Miyata, S., *Anion-exchange properties of hydrotalcite-like compounds.* Clays and Clay minerals, 1983. **31**(4): p. 305-311.
35. Luo, R., et al., *Study of chloride binding and diffusion in GGBS concrete.* Cement and Concrete Research, 2003. **33**(1): p. 1-7.
36. Puertas, F., et al., *Alkali-activated fly ash/slag cements: strength behaviour and hydration products.* Cement and concrete research, 2000. **30**(10): p. 1625-1632.
37. Kumar, S., R. Kumar, and S. Mehrotra, *Influence of granulated blast furnace slag on the reaction, structure and properties of fly ash based geopolymer.* Journal of materials science, 2010. **45**(3): p. 607-615.
38. Yang, T., et al., *Mechanical property and structure of alkali-activated fly ash and slag blends.* Journal of Sustainable Cement-Based Materials, 2012. **1**(4): p. 167-178.
39. Zhu, H., et al., *Durability of alkali-activated fly ash concrete: chloride penetration in pastes and mortars.* Construction and Building Materials, 2014. **65**: p. 51-59.
40. Lloyd, R.R., et al., *Spatial distribution of pores in fly ash-based inorganic polymer gels visualised by Wood's metal intrusion.* Microporous and Mesoporous Materials, 2009. **126**(1-2): p. 32-39.
41. Xie, J., et al., *Effects of combined usage of GGBS and fly ash on workability and mechanical properties of alkali activated geopolymer concrete with recycled aggregate.* Composites Part B: Engineering, 2019. **164**: p. 179-190.
42. Lee, N. and H.-K. Lee, *Influence of the slag content on the chloride and sulfuric acid resistances of alkali-activated fly ash/slag paste.* Cement and concrete composites, 2016. **72**: p. 168-179.
43. Ismail, I., et al., *Drying-induced changes in the structure of alkali-activated pastes.* Journal of Materials Science, 2013. **48**(9): p. 3566-3577.
44. Garanayak, L., *Behavior of alkali activated fly ash slag paste at room temperature.* Materials Today: Proceedings, 2020.
45. *ASTM C305-14, Standard practice for mechanical mixing of hydraulic cement pastes and mortars of plastic consistency* ASTM 2003: American Society for Testing and Materials (ASTM), West Conshohocken, PA.
46. Allahverdi, A., E.N. Kani, and M. Yazdanipour, *Effects of blast-furnace slag on natural pozzolan-based geopolymer cement.* Ceramics-Silikáty, 2011. **55**(1): p. 68-78.
47. Standard, A., *ASTM C109-standard test method for compressive strength of hydraulic cement mortars.* ASTM International, West Conshohocken, PA, 2008.
48. Liu, C., X. Gao, and Y. Zhou, *Research on hydration mechanism of slag composite cementitious material mixed with NaCl.* Journal of Chemical and Pharmaceutical Research, 2014. **6**(4): p. 845-849.
49. Liu, C., H. Ji, and J. Liu, *Characteristics of slag fine-powder composite cementitious material-cured coastal saline soil.* Emerging Materials Research, 2014. **3**(6): p. 282-291.
50. Liu, J., et al., *Effects of w/b ratio, fly ash, limestone calcined clay, seawater and sea-sand on workability, mechanical properties, drying shrinkage behavior and micro-structural characteristics of concrete.* Construction and Building Materials, 2022. **321**: p. 126333.
51. Noushini, A. and A. Castel, *The effect of heat-curing on transport properties of low-calcium fly ash-based geopolymer concrete.* Construction and Building Materials, 2016. **112**: p. 464-477.
52. Sindhunata, et al., *Effect of curing temperature and silicate concentration on fly-ash-based geopolymerization.* Industrial & Engineering Chemistry Research, 2006. **45**(10): p. 3559-3568.
53. Sajan, P., et al., *Combined effect of curing temperature, curing period and alkaline concentration on the mechanical properties of fly ash-based geopolymer.* Cleaner Materials, 2021. **1**: p. 100002.

54. Kantarci, F., İ. Türkmen, and E. Ekinci, *Influence of various factors on properties of geopolymer paste: A comparative study.* Structural Concrete, 2020.
55. Ranjbar, N., et al., *Compressive strength and microstructural analysis of fly ash/palm oil fuel ash based geopolymer mortar under elevated temperatures.* Construction and building materials, 2014. **65**: p. 114-121.
56. Rajarajeswari, A. and G. Dhinakaran, *Compressive strength of GGBFS based GPC under thermal curing.* Construction and Building Materials, 2016. **126**: p. 552-559.
57. Chindaprasirt, P. and U. Rattanasak, *Characterization of the high-calcium fly ash geopolymer mortar with hot-weather curing systems for sustainable application.* Advanced Powder Technology, 2017. **28**(9): p. 2317-2324.
58. Bakharev, T., *Geopolymeric materials prepared using Class F fly ash and elevated temperature curing.* Cement and concrete research, 2005. **35**(6): p. 1224-1232.
59. Chi, M., *Effects of dosage of alkali-activated solution and curing conditions on the properties and durability of alkali-activated slag concrete.* Construction and Building Materials, 2012. **35**: p. 240-245.
60. Lemougna, P.N., K.J. MacKenzie, and U.C. Melo, *Synthesis and thermal properties of inorganic polymers (geopolymers) for structural and refractory applications from volcanic ash.* Ceramics International, 2011. **37**(8): p. 3011-3018.
61. Takeda, H., et al., *Fabrication and characterization of hardened bodies from Japanese volcanic ash using geopolymerization.* Ceramics International, 2014. **40**(3): p. 4071-4076.
62. Djobo, J.N.Y., et al., *Volcanic ash-based geopolymer cements/concretes: the current state of the art and perspectives.* Environmental Science and Pollution Research, 2017. **24**(5): p. 4433-4446.
63. Phoo-ngernkham, T., et al., *Effects of sodium hydroxide and sodium silicate solutions on compressive and shear bond strengths of FA–GBFS geopolymer.* Construction and Building Materials, 2015. **91**: p. 1-8.
64. Burciaga-Díaz, O. and J.I. Escalante-García, *Structure, mechanisms of reaction, and strength of an alkali-activated blast-furnace slag.* Journal of the American Ceramic Society, 2013. **96**(12): p. 3939-3948.
65. Haha, M.B., et al., *Influence of activator type on hydration kinetics, hydrate assemblage and microstructural development of alkali activated blast-furnace slags.* Cement and Concrete Research, 2011. **41**(3): p. 301-310.
66. Myers, R.J., et al., *Generalized structural description of calcium–sodium aluminosilicate hydrate gels: the cross-linked substituted tobermorite model.* Langmuir, 2013. **29**(17): p. 5294-5306.
67. Lee, N., J.G. Jang, and H.-K. Lee, *Shrinkage characteristics of alkali-activated fly ash/slag paste and mortar at early ages.* Cement and Concrete Composites, 2014. **53**: p. 239-248.
68. Lemougna, P.N., et al., *Effect of slag on the improvement of setting time and compressive strength of low reactive volcanic ash geopolymers synthetized at room temperature.* Materials Chemistry and Physics, 2020. **239**: p. 122077.
69. Jin, F., K. Gu, and A. Al-Tabbaa, *Strength and drying shrinkage of reactive MgO modified alkali-activated slag paste.* Construction and Building Materials, 2014. **51**: p. 395-404.
70. Jun, Y., S. Yoon, and J.E. Oh, *A comparison study for chloride-binding capacity between alkali-activated fly ash and slag in the use of seawater.* Applied Sciences, 2017. **7**(10): p. 971.
71. Shi, Z., et al., *Role of calcium on chloride binding in hydrated Portland cement–metakaolin–limestone blends.* Cement and Concrete Research, 2017. **95**: p. 205-216.
72. Li, F., et al., *Physical and mechanical properties and micro characteristics of fly ash-based geopolymer paste incorporated with waste Granulated Blast Furnace Slag (GBFS) and functionalized Multi-Walled Carbon Nanotubes (MWCNTs).* Journal of Hazardous Materials, 2020. **401**: p. 123339.
73. Zhang, P., et al., *Self-cementation solidification of heavy metals in lead-zinc smelting slag through alkali-activated materials.* Construction and Building Materials, 2020. **249**: p. 118756.

74. Xia, M., et al., *Solidification/stabilization of lead-zinc smelting slag in composite based geopolymer.* Journal of Cleaner Production, 2019. **209**: p. 1206-1215.
75. Ranjbar, N., et al., *Effects of heat and pressure on hot-pressed geopolymer.* Construction and Building Materials, 2020. **231**: p. 117106.
76. Fernández-Jiménez, A., et al., *Alkaline activation of metakaolin–fly ash mixtures: obtain of zeoceramics and zeocements.* Microporous and mesoporous materials, 2008. **108**(1-3): p. 41-49.